



DeepMIP-Eocene-p2: Experimental design for Phase 2 of the early Eocene component of the the CMIP7/PMIP7 Deep-time Model Intercomparison Project (DeepMIP-Eocene)

Daniel J. Lunt¹, Nicky M. Wright², Bram Vaes³, Ulrich Salzmann⁴, James W. B. Rae⁵, Thomas Hickler⁶, David K. Hutchinson⁷, Julia Brugger⁸, Jiang Zhu⁹, Sebastian Steinig¹, A. Nele Meckler¹⁰, Gordon N. Inglis¹¹, David Evans¹¹, Agatha M. de Boer¹², Bette L. Otto-Bliesner⁹, Natalie Burls¹³, Yurui Zhang¹⁴, Appy Sluijs¹⁵, Tammo Reichgelt¹⁶, Igor Niezgodzki¹⁷, Katrin Meissner⁷, Jean-Baptiste Ladant¹⁸, Fanni D. Kelemen¹⁹, Matthew Huber²⁰, David Greenwood²¹, Mattias Green²², Flavia Boscolo-Galazzo²³, Manuel Tobias Blau²⁴, and Michiel Baatsen²⁵

¹School of Geographical Sciences, University of Bristol, UK

²EarthByte Group, School of Geosciences, The University of Sydney, Australia

³Department of Earth and Environmental Sciences, University of Milano-Bicocca

⁴School of Geography and Natural Sciences, Northumbria University, Newcastle upon Tyne, UK

⁵School of Earth and Environmental Sciences, University of St Andrews, UK

⁶Senckenberg Biodiversity and Climate Research Centre, Germany; Department of Physical Geography, Geosciences, Goethe University, Frankfurt am Main, Germany

⁷Climate Change Research Centre, University of New South Wales, Sydney, NSW, Australia

⁸Geo- and Environmental Research Center, University of Tübingen, Germany

⁹Climate and Global Dynamics Laboratory, NSF National Center for Atmospheric Research, Boulder, 80305, USA

¹⁰Department of Earth Science, Bjerknes Centre for Climate Research, Bergen, Norway

¹¹School of Ocean and Earth Science, University of Southampton, UK

¹²Department of Geological Sciences, Stockholm University, Sweden

¹³Atmospheric, Oceanic and Earth Sciences Department, George Mason University, USA

¹⁴Department of Geological Oceanography, Xiamen University, China

¹⁵Department of Earth Sciences, Utrecht University, Netherlands

¹⁶Department of Earth Sciences, University of Connecticut, USA

¹⁷Institute of Geological Sciences, Polish Academy of Sciences, Poland

¹⁸Laboratoire des Sciences du Climat et de l'Environnement, LSCE/IPSL, CEA-CNRS-UVSQ, Université Paris-Saclay, Gif-sur-Yvette, France

¹⁹Institute for Atmospheric and Environmental Sciences, Goethe University Frankfurt, Germany

²⁰Department of Earth, Atmospheric, and Planetary Sciences, Purdue University, USA

²¹Department of Biology, Brandon University, Canada

²²School of Ocean Sciences, Bangor University, UK

²³MARUM, University of Bremen, Bremen, Germany

²⁴School of Earth and Environmental Sciences, Seoul National University, Seoul 08826, South Korea

²⁵IMAU, Utrecht University, Department of Physics, Utrecht, The Netherlands

Correspondence: Daniel J. Lunt (d.j.lunt@bristol.ac.uk)

Abstract. Warm, high-CO₂ climates of Earth's past provide an opportunity to evaluate climate models under extreme forcing, and to explore mechanisms that lead to such warmth. One such time period is the early Eocene, when global mean surface temperatures were 10–17 °C higher than preindustrial, and CO₂ concentrations were ~1500 ppmv. In this paper we present the



experimental design for Phase 2 of the Eocene component of the Deep-time Model Intercomparison project (DeepMIP-Eocene-5 p2). The aim is to provide a framework for modelling groups to carry out a common set of simulations, thereby facilitating exploration of inter-model dependencies. The focus is on the early Eocene Climatic Optimum (EECO, ~53.3-49.1 million years ago). Relative to Phase 1 of DeepMIP-Eocene, we provide a new paleogeography (topography, bathymetry) derived from several recent independent reconstructions that focused on different regions, a new vegetation derived by merging paleobotanical data with vegetation model simulations, and a new CO₂ specification derived from recent reevaluations of proxy data. The 10 core set of simulations consists of a preindustrial control, an abrupt increase to 4× preindustrial CO₂ concentrations from this preindustrial control, a standard control EECO simulation at 5× preindustrial CO₂ concentrations, and an EECO simulation with preindustrial CO₂ concentrations. In addition to these core simulations, we suggest a suite of optional sensitivity studies, which allow the impact of various factors to be explored, such as topography/bathymetry, greenhouse gases, land-surface parameters, astronomical and solar forcings, and internal model parameters. The updated boundary conditions and guidance on 15 initialisation and spinup in Phase 2 will allow more robust model-data comparisons, more accurate insights into mechanisms influencing early Eocene climate, and increased relevance for informing future climate change projections.

1 Introduction

The study of paleoclimates, and in particular the study of paleoclimates using climate models, generally has two main motivations. First, to study the past climate of our Earth from a purely ‘blue-skies’ desire to better understand the planet that we 20 live on – because, as George Mallory reportedly said in regard to climbing Mount Everest, “it is there” (Rak, 2021). Second, to leverage information from Earth’s past climates in order to better understand and predict future climates, so to inform political decisions regarding climate-related policy and to enable society to better adapt to future climate change. The Deep-time Modelling Intercomparison Project (DeepMIP) is driven by these two motivations, and is dedicated to conceiving, designing, carrying out, analysing, and disseminating, an international effort to improve our understanding of Deep Time climates. ‘Deep-time’ is here defined as any time period older than the Pliocene period, i.e. older than 5.3 million years ago. The objectives of 25 DeepMIP are:

- to foster closer links between the palaeoclimate modelling and data communities,
- to design experiments for the MIP, through discussion with both model and data communities,
- to carry out such simulations with a wide range of models,
- to create, collate, and synthesise datasets where appropriate to enable meaningful model-data comparisons,
- to analyse the results with the aims of evaluating the models, understanding the reasons behind the model-model and model-data differences, and, where possible, providing suggestions for model improvements, and
- to carry out the above in such a way as to facilitate contribution to the Intergovernmental Panel on Climate Change (IPCC).



35 DeepMIP is a part of the Paleoclimate Modelling Intercomparison Project (PMIP), which itself is a part of the Coupled Model Intercomparison Project (CMIP), which is a project of the World Climate Research Program (WCRP). Together with the Pliocene Model Intercomparison (PlioMIP) effort (Haywood et al., 2024), DeepMIP-Eocene (Lunt et al., 2021) and DeepMIP-Miocene (Burls et al., 2021) extend PMIP efforts back beyond the Quaternary, to sample the full range of paleoclimate states that are comparable, at least in terms of CO₂ concentration, with the projected Shared Socioeconomic Pathways (SSPs; Mein-40 shausen et al., 2020).

Here, in preparation for CMIP7/PMIP7 (Dunne et al., 2025), we focus on the Eocene component of DeepMIP: DeepMIP-Eocene. The Eocene (56.0 to 33.9 million years ago), is a geological epoch that is characterised by a substantially warmer climate than modern (Figure 1). Within the Eocene, much previous focus in DeepMIP has been on the early Eocene Climatic Optimum (EECO); ~53.3-49.1 million years ago (Hollis et al., 2019). Proxies indicate global mean near-surface temperatures about 10-17 °C higher than preindustrial (Inglis et al., 2020a; Evans et al., 2024), CO₂ concentrations of ~1500 ppmv (Anagnostou et al., 2020, see also Section 2.2.1), and no ice sheets. Proxies indicate wetter high latitudes than modern (Cramwinckel et al., 2023; West et al., 2020), and a vegetation consistent with a generally warmer and wetter climate than modern, including a poleward expansion of temperate and warm-temperate forests in regions today covered by tundra shrub and boreal forests (Thompson et al., 2025). In the context of the Phanerozoic (last 540 million years), the paleogeography at this time was relatively similar to today, with distinct Atlantic, Indian, and Pacific oceans, and with the modern continents recognisable in terms of their relative positioning (see Figure 3). However, the paleogeography differed from the modern in several respects, including an open Panama Seaway, constricted Tasman seaway and Drake passage, an open Tethys seaway, India disconnected from southeast Asia, and changes to the heights and configurations of multiple mountain ranges (Herold et al., 2014). Despite these differences in paleogeography, the climate of the early Eocene has been compared to possible future climates under very high emissions scenarios (Burke et al., 2018; Arias et al., 2021), and has been used to constrain Equilibrium Climate Sensitivity (ECS, e.g. Forster et al., 2021; Inglis et al., 2020a). As such, the EECO provides a window to a substantially warmer world than today. It provides an opportunity to evaluate models, to use models to inform the interpretation of proxy records, and to provide mechanistic understanding of climate feedbacks in a warm world.

The first phase of DeepMIP-Eocene was based around a model experimental design in which paleogeography, CO₂, and vegetation boundary conditions were prescribed (Lunt et al., 2017), informed to a large extent by the work of Herold et al. (2014). Eight modelling groups submitted simulations to the first phase, the results from which are available in the DeepMIP model dataset (Steinig et al., 2024), and have been discussed in multiple studies, which are summarised very briefly here. Lunt et al. (2021) presented an overview of the large-scale temperatures, partitioning the modelled global mean surface temperature (GMST) and temperature gradients to different mechanisms through an energy-balance analysis, finding that a subset of the models showed results that were consistent with the proxies in terms of GMST, temperature gradient, and CO₂, and finding that non-CO₂ boundary conditions contributed between 3-5 °C to Eocene warmth. Kelemen et al. (2023) found that these non-CO₂ boundary conditions also played a key role in the meridional heat transport, leading to more heat transported to the South Pole by the ocean, and more heat transported northwards in the northern mid-latitudes by transient atmospheric eddies. Goudsmit-Harzevoort et al. (2023) found a strong 1-1 coupling between deep ocean and surface air temperature change across

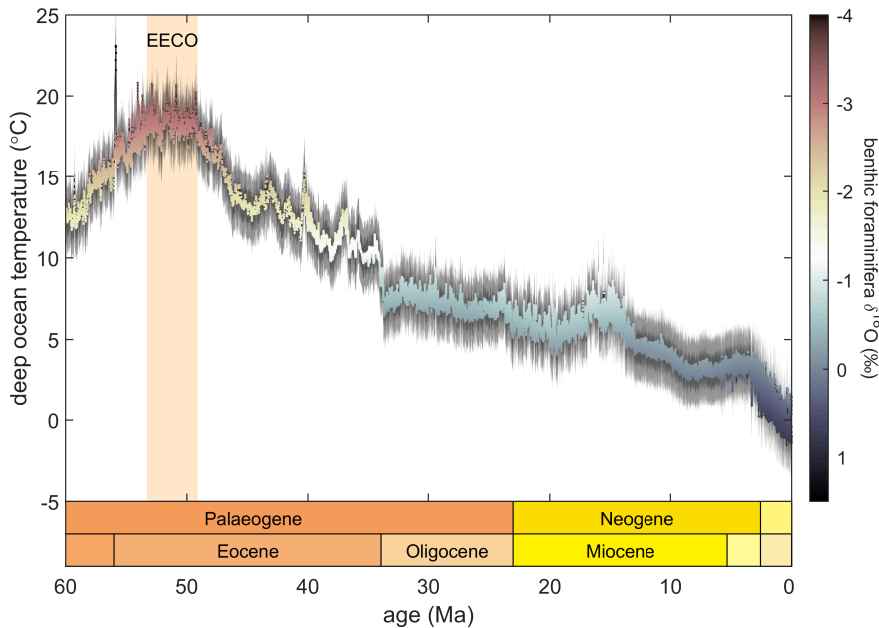


Figure 1. Deep ocean temperature through the Cenozoic, derived from the $\delta^{18}\text{O}$ of benthic foraminifera (Evans et al., 2024). The early Eocene Climatic Optimum (EECO; \sim 53.3-49.1 million years ago as defined by Hollis et al. (2019)) is highlighted, which is the focus of DeepMIP-Eocene Phase 2.

70 the ensemble, and found a best fit with deep ocean temperature proxies at $6\times$ preindustrial CO_2 concentrations. Evans et al. (2024) supported this finding, indicating that changes in deep ocean temperatures in general correlate well with changes in surface temperature. Cramwinckel et al. (2023) explored the large-scale modelled hydrology, finding a thermodynamically-dominated hydrological response leading to wetting in the mid and high latitudes, and drier conditions in the subtropics, and wetting in the deep tropics, and finding that those models with the weakest meridional temperature gradients were in 75 best agreement with precipitation proxies. Regional precipitation patterns and model-data comparisons were explored in Africa by Williams et al. (2022) and in Australia by Reichgelt et al. (2022). Both these studies estimated the CO_2 concentration for which the model simulations best agreed with the proxy vegetation data, with Reichgelt et al. (2022) finding best agreement at $6\times$, in contrast to Williams et al. (2022) who found best agreement at much lower values (as low as $1\times$). Abhik et al. (2024) showed that the modelled early Eocene Asian wet season was weaker than present day in the ensemble, and attributed this 80 to the reduced Tibetan Plateau, and that this dominated over the response to the CO_2 forcing. Furthermore, by carrying out additional paleogeographic sensitivity studies, Zhang et al. (2022) showed that the East Asian precipitation was determined to a large extent by the Southeast Mountains. Meijer et al. (2024) showed that proxies indicate monsoonal precipitation in the Asian continental interior during the early Eocene, but that this is not reproduced to such an extent in the DeepMIP-Eocene model results. Zhang et al. (2022) found that all the models were dominated by strong deepwater formation in the Southern Ocean, 85 at locations determined by Southern Ocean gateway geometry, but that one model also showed strong deepwater formation



in the North Pacific, and that two models also showed deepwater formation in the North Atlantic. In the Pacific, there was a northward migration of the subtropical gyre, as evidenced in DeepMIP-Eocene models and the sedimentary record (Zhang et al., 2025). The lack of direct evidence of sea ice in the Eocene, coupled with the presence of subtropical taxa (e.g. Willard et al., 2019) and extensive temperature forest (e.g. West et al., 2020) in the Eocene Arctic, means that model simulations with 90 extensive EECO sea ice are problematic to reconcile with the proxy record. In this context, Niegzodzki et al. (2022) investigated modelled sea ice during the Eocene, finding that the CO₂ threshold for formation of Arctic ice was very model dependent, and that implementation of river run-off and ocean basin connections were important for determining these model differences.

Although these studies arising from Phase 1 of DeepMIP-Eocene have considerably advanced our understanding of Eocene climate, there are some aspects of the experimental design which mean that uncertainties remain. For example, the paleogeography and vegetation boundary conditions which were prescribed in the Phase 1 model simulations have been superseded by 95 more recent reconstructions (see Section 2.2.2), and the standard CO₂ concentration of 840 ppmv is low compared with recent proxy reconstructions (see Section 2.2.1). Also, the recommended initial condition for the ocean temperature had an unrealistic vertical profile, and as a result many models did not reach full equilibrium by the end of their simulations. In addition, models 100 themselves have improved since Phase 1, and computing power has increased, meaning that more advanced models could be used. It is therefore timely to define a new set of recommended boundary conditions to allow a Phase 2 of DeepMIP-Eocene.

In this paper we describe boundary conditions and experimental protocols for DeepMIP-Eocene Phase 2 (DeepMIP-Eocene-p2). Section 2.1 describes the choice of time period and core simulations, Section 2.2 describes the boundary conditions, Section 2.3 includes suggestions for sensitivity studies, Section 2.4 describes the initialisation and stabilisation protocols, and Section 2.5 describes the format for model outputs. The paper concludes with a summary and plans for future analyses (Section 105 3).

2 Experimental Design

2.1 Choice of time periods, overview of experimental design, and simulation list

In the experimental design for DeepMIP-Eocene Phase 1 (Lunt et al., 2017), three periods within the Paleocene/Eocene were explicitly identified for study - the Paleocene-Eocene Thermal Maximum (PETM), the latest Paleocene or pre-PETM, and the 110 EECO. These corresponded to the same three periods for which data compilations were presented in Hollis et al. (2019) and Inglis et al. (2020a), which were defined as representing 56 Ma, 57-56 Ma, and 53.3-49.1 Ma, respectively. However, model simulations for these periods differed solely in their prescribed CO₂ concentration, and the paleogeography used was originally designed to be most appropriate for 55 Ma. Subsequent analyses of model results, and model-data comparisons, tended to focus on the EECO. In Phase 2 we decide to focus solely on the EECO, 53.3-49.1 Ma.

115 The paleogeography and vegetation boundary conditions for Phase 2 have been updated from Phase 1, as described in detail in Sections 2.2.2 and 2.2.3 respectively, and we provide the appropriate boundary conditions as NetCDF files on Zenodo Lunt (2025b).



120 The CO₂ boundary condition is discussed in more detail in Section 2.2.1; in summary, we follow Phase 1 in suggesting sensitivity simulations at multiple CO₂ concentrations (see Section 2.3), but increase the ‘standard’ CO₂ from 3× preindustrial CO₂ concentrations (3×PI) to 5×PI, to be more in line with recent CO₂ proxies.

125 The primary EECO boundary conditions described in Section 2.2 define the standard DeepMIP-Eocene Phase 2 simulation (*deepmip-p2-stand-5xCO2*, Table 1). In addition, the analysis of the DeepMIP-Eocene Phase 1 ensemble benefited greatly from the existence of a preindustrial control (simulation *piControl*, Table 1) and an Eocene simulation at 1×PI (simulation *deepmip-p2-stand-1xCO2*, Table 1), which allowed anomalies relative to preindustrial and the contribution of non-CO₂ forcings to be readily identified. As such, we retain these simulations in Phase 2, and make the 1×PI Eocene simulation mandatory.

130 Assessment of the relevance of the simulations for constraining ECS, for example through emergent constraints, was hampered by the absence of an instantaneous modern 4×PI simulation for many models. As such, we make this simulation mandatory in Phase 2 (*abrupt-4xCO2*, Table 1), allowing the ECS of every model to be calculated robustly and consistently across the model ensemble. The standard length of this ECS-determining simulation is relatively short at 150 years, and will likely already exist for some models as it is a core simulation in the ‘DECK’ of CMIP7 (Dunne et al., 2025), and as such it should not represent a substantial computational burden. Some models may use different internal model parameters in their standard modern and Eocene configurations (e.g. differences in background vertical diffusivity). In this case, it should be clearly documented which version of the model the *abrupt-4xCO2* simulation, and the associated preindustrial control, are carried out with (or, ideally, both versions should be used).

135 Other aspects to be explored in sensitivity studies, depending on the resources available, include paleogeography, vegetation, and the prescribed solar luminosity and methane (see Section 2.3).

A list of all the mandatory simulations (in bold), and suggested sensitivity studies, is given in Table 1.

2.2 Boundary Conditions for Eocene simulation *deepmip-p2-stand-5xCO2*

140 Here we define the boundary conditions for the standard DeepMIP-Eocene Phase 2 simulation (*deepmip-p2-stand-5xCO2*), including CO₂ (Section 2.2.1), paleogeography (Section 2.2.2), and vegetation (Section 2.2.3). Other boundary conditions, which are unchanged since Phase 1, are described briefly in Section 2.2.4, with references given to the more detailed explanations in Lunt et al. (2017).

2.2.1 CO₂ Boundary Condition

145 For atmospheric CO₂, we make use of the ‘smoothed’ CO₂ of Hönisch et al. (2023), which is a community-endorsed CO₂ record based on multiple proxies. This compilation is considerably updated and expanded from the boron isotope-based record of Anagnostou et al. (2016) that was available at the time of Phase 1. Averaged over the period of the EECO (53.3–49.1 Ma), the Hönisch et al. (2023) record has a value of 1380 ppmv (4.9×PI; dashed horizontal black line, Figure 2). As such, we define the DeepMIP-Eocene Phase 2 CO₂ as 5×PI, i.e. 1400 ppmv (red solid horizontal line, Figure 2). This is substantially higher than the 3×PI that was the standard in DeepMIP-Eocene Phase 1 (dashed horizontal magenta line, Figure 2). The value of 150 5×PI is also supported by the compilation of Rae et al. (2021), which is based on boron isotopes, taking account of changes in

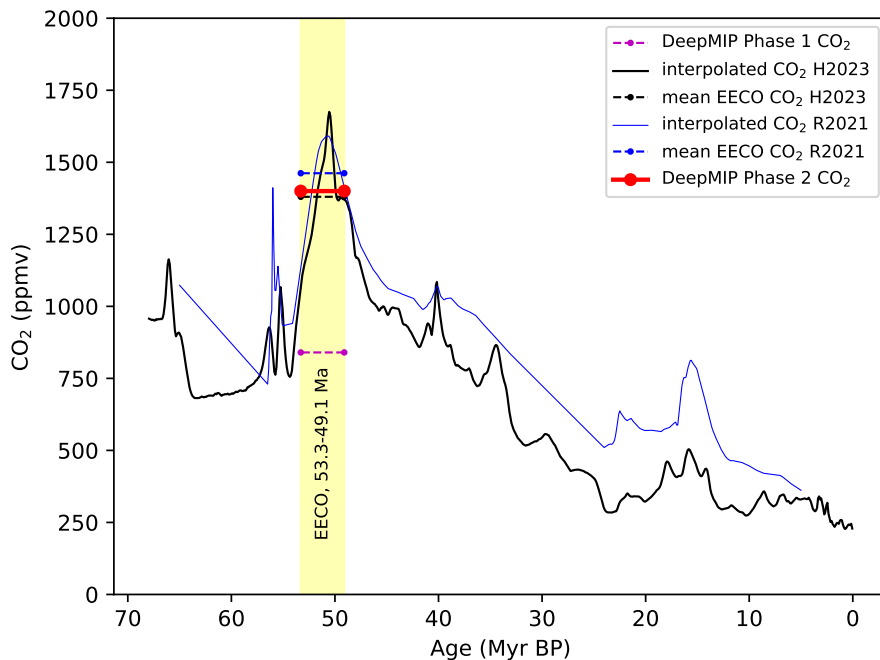


Figure 2. Construction of the standard DeepMIP-Eocene Phase 2 CO₂ concentration. Black solid line shows the Hönisch et al. (2023) (H2023) CO₂ record. Blue solid line shows the Rae et al. (2021) (R2021) CO₂ record. Black and blue dashed lines shows the respective means of the H2023 and R2021 records over the EECO period, 53.3 to 49.1 Ma. Red solid line shows the DeepMIP-Eocene Phase 2 CO₂ of 1400 ppmv (5×PI). Magenta dashed line shows the standard CO₂ concentration in DeepMIP-Eocene Phase 1 (3×PI).

the boron isotopic concentration of seawater over time, and alkenone carbon isotopes. The loess-smoothed version of Rae et al. (2021) (their Figure 6), linearly interpolated to a 0.1 Myr timescale, and then averaged over the EECO (dashed horizontal blue line, Figure 2), is 1462 ppmv for the EECO, which is about 5.2×PI (although we note that there is substantial overlap between the Hönisch et al. (2023) and Rae et al. (2021) records over the period of the EECO, so the similarity between them is not unexpected). A value of 5×PI is further supported by the fact that the simulations with the best agreement with temperature proxies (GMST and meridional temperature gradient) in Phase 1 were all in the range 4×PI to 6×PI (Lunt et al., 2021).

We note that CO₂ of 5×PI under Eocene conditions may lead to crashes or runaway for some models (Lunt et al., 2021; Zhu et al., 2024). In this case, we encourage the modelling groups to apply the highest CO₂ their model can use in order to have a stable simulation (typically assessed by the surface and/or deep ocean temperature trends, and top-of-model net radiation; see Section 2.4). In addition, we encourage the modelling groups to report the CO₂ and temperature levels at which the model crashes frequently or ‘runs away’.

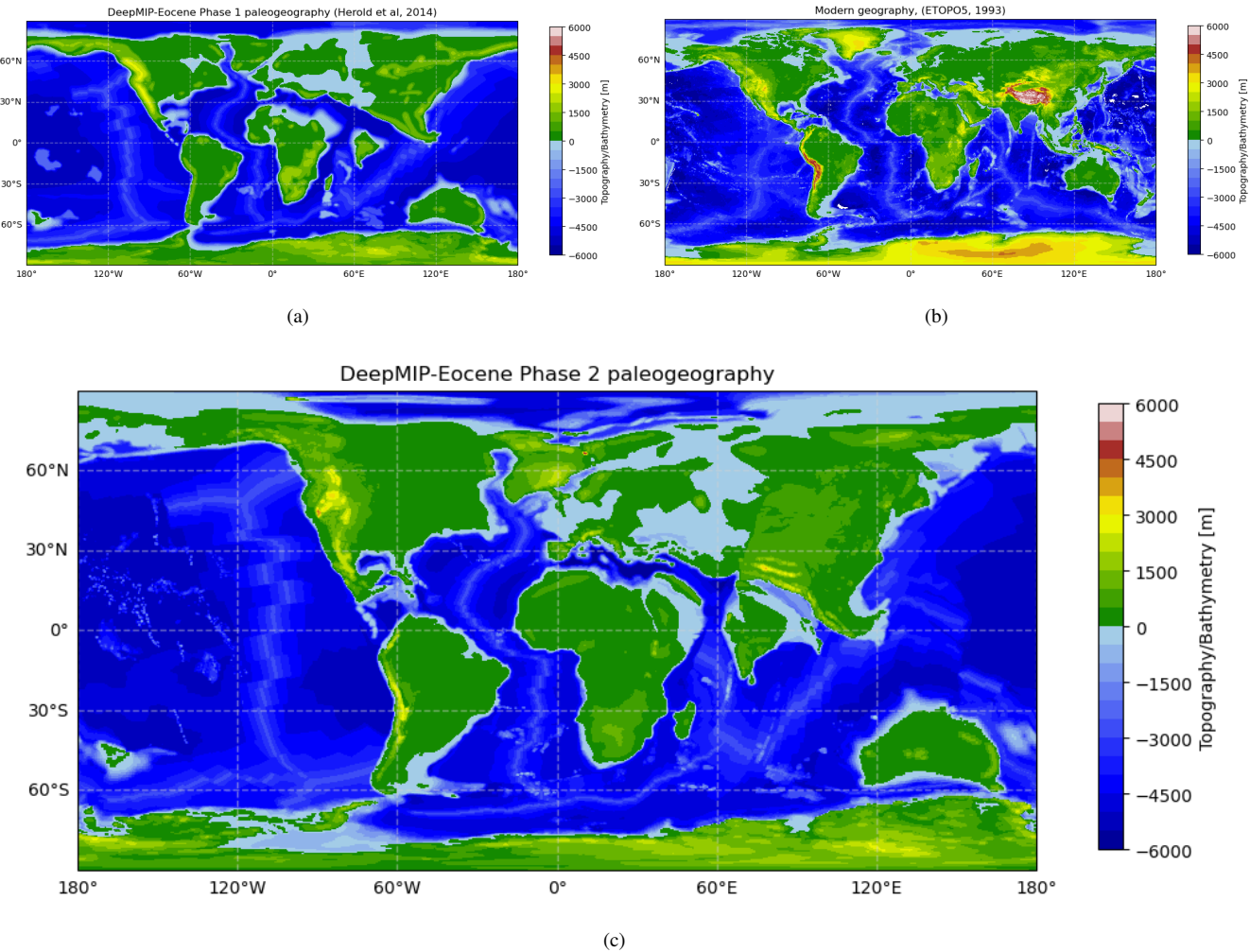


Figure 3. (a) The Herold et al. (2014) paleogeography used in DeepMIP-Eocene Phase 1. (b) The modern geography from ETOPO5 (National Geophysical Data Center, 1993). (c) The DeepMIP-Eocene Phase 2 paleogeography, which is a combination of Herold et al. (2014), Scotese and Wright (2018), He et al. (2019), and Straume et al. (2020).

2.2.2 Paleogeography Boundary Conditions

The paleogeography (including land-sea mask) used in DeepMIP-Eocene Phase 1 was that of Herold et al. (2014), shown in Figure 3a. This paleogeographic reconstruction was an update of Markwick (2007) and relied on the global plate tectonic model of Müller et al. (2008) placed in the mantle (specifically, hotspot) frame of O'Neill et al. (2005). Files were also provided for the same paleogeography, but placed in the paleomagnetic reference frame of Torsvik et al. (2012), and an independent second paleogeography was provided by Getech Plc.



For Phase 2, we provide a fully updated paleogeography that builds on recent advances and updates in paleogeographic reconstruction of the Eocene. Since 2014, several studies published new paleogeographic reconstructions for the early Eocene, 170 including Scotese and Wright (2018), He et al. (2019), Straume et al. (2020) with minor updates in Straume et al. (2024), and Aminov et al. (2023). Although these reconstructions are global, the authors often focused on specific regions that were reconstructed in more detail, while other regions were left unchanged from earlier work or simply retained their present-day topography (see Appendix, Figure A1). Given the different methods and underlying data used to construct them, it is problematic to assess which reconstruction is ‘best’. Here, we take a pragmatic approach and integrate the most detailed 175 paleogeographic reconstructions per continent in a new paleogeography for the early Eocene (51 Ma).

As a basis, we use the global plate model of Zahirovic et al. (2022) placed in a paleomagnetic reference frame (anchored plate ID = 701701). This plate reconstruction is the current default model in the widely used GPlates software Müller et al. (2018) and is the same as that being used in DeepMIP-Miocene Phase 2 (Burls et al., in prep). The paleomagnetic reference frame is from Merdith et al. (2021), based on the approach outlined in Tetley et al. (2019). We account for differences in the 180 underlying plate tectonic model of each paleogeography reconstruction used here by rotating them, prior to their incorporation, into the Zahirovic et al. (2022) plate model (and associated reference frame) at 51 Ma.

We have integrated different regional reconstructions as follows. We incorporate global paleobathymetry at 51 Ma using the method described in Wright et al. (2020) applied to the Zahirovic et al. (2022) plate model (including paleo-oceanic age grid) to ensure self-consistency. For Antarctica, we adopt the ‘maximum’ topographic reconstruction for 34 Ma (Eocene-Oligocene 185 boundary) from Paxman et al. (2019), which provides an update of the ANTscape reconstruction for 34 Ma (Wilson et al., 2012) used in Herold et al. (2014). We retain the reconstruction of Australia and Zealandia from Herold et al. (2014) and preserve the reconstruction of the southern hemisphere gateways of Phase 1, as in Herold et al. (2014). This means that both the Drake Passage and Tasman Gateways are open but shallow, preventing any deepwater throughflow. For South America and the Caribbean region, we rely on the reconstruction of Aminov et al. (2023) for 50 Ma, except for the Andes, where we use the 190 detailed reconstruction from Boschman (2021). We include an updated version of the 50 Ma reconstruction of Aminov et al. (2023) for India and eastern Asia, that includes a more realistic position of the Burma terrane and extent of Greater India based on the India-Asia collision scenario of Westerweel et al. (2025). The reconstruction of the Tibetan region, with its three narrow mountain ranges and intermontane valleys, corresponds to the early Eocene paleo-elevation model of Spicer et al. (2025). For Africa and North America, we integrate the recently published reconstruction of Montheil et al. (2026), which builds upon the 195 work of Poblete et al. (2021) and Aminov et al. (2023). The African topography reflects the middle Eocene (48-41 Ma) and is based on the paleo-facies maps of Couvreur et al. (2021). For North America, Montheil et al. (2026) modified the earlier early-middle Eocene reconstructions that included a long, 4-km-high plateau in the North American Cordillera, producing a more realistic topography. Finally, we adopt the reconstruction of Straume et al. (2020, 2024) for the western Tethyan region, 200 western Eurasia and the Arctic (including Greenland). These authors provided a detailed study of the northern hemisphere gateways: in this reconstruction, there is no connection between the Arctic and Pacific Oceans, as well as between the Arctic and Labrador Sea. The Arctic Ocean is connected to the Neo-Tethys through the West Siberian Seaway (Straume et al., 2024). We include a shallow connection between the Arctic and Atlantic Oceans through the Barents Sea, Norwegian Sea, and North



Sea. This represents a maximum connectivity scenario for 50-48 Ma with water exchange between the northeast Atlantic and Arctic, supported by the widespread occurrence of the *Azolla* fern in the Arctic and Nordic seas (Brinkhuis et al., 2006).

205 As in Phase 1, the land-sea mask is defined as the zero contour of the paleogeography. As the paleogeographic reconstructions used here all have modified the paleo-coastlines after sea level corrections, we do not make an additional explicit sea level correction during our merging process. One exception here is for the Paxman et al. (2019) Antarctica paleotopography, which is reconstructed relative to modern-day sea level—here we incorporate a sea level adjustment based on Wright et al. (2020). We made minor adjustments to regions where two paleogeographic reconstructions were merged, to avoid artifacts such as sudden
210 jumps in topography or bathymetry. In addition, we removed most interior lakes/seas and very small islands to minimize the manual adjustments needed after re-gridding the map to model resolution.

215 The resulting DeepMIP-Eocene Phase 2 paleogeography is shown in Figure 3b, and provided as a NetCDF file on Zenodo Lunt (2025b). The map is provided at a relatively high resolution of $0.25^\circ \times 0.25^\circ$ (compared to $1^\circ \times 1^\circ$ in Phase 1), to allow high resolution atmosphere-only simulations to be carried out (see Section 2.3.4), and to allow sub-gridscale topography to be calculated (see below).

220 Besides the switch to a paleomagnetic reference frame, the main difference between the Phase 2 paleogeography and that of Herold et al. (2014) is that the continental interiors are generally lower in the Phase 2 topography. This is because Herold et al. (2014) built upon the reconstruction of Markwick (2007), whose reconstruction approach generated some anomalously high plateaus in continental interiors. This becomes evident from the fact that the Herold et al. (2014) Eocene topography is substantially higher (in places $>1\text{km}$) than modern in the Rockies, India, southern Africa, and much of southeast Asia (see Appendix, Figure A1). Another important difference is the reduced width of the Neo-Tethys Ocean. This follows from the change of the reconstruction age from 55 to 51 Ma, during which Africa and particularly India have moved farther north relative to Eurasia. There are also changes in the extent of shallow seas, with a reduction in northern Afro-Arabia in Phase 2 compared with Phase 1, and an increase north of India. Correct representation of these shelves could be particularly important for models
225 which incorporate biogeochemistry. There is a more detailed representation of small-scale island features, in particular in the Tethys, which could be important for correctly representing flow through gateways in models with high resolution in the ocean.

230 For some lower-resolution models, some ocean gateways may not be fully resolved, resulting in them being closed or shallow when they should be open or deep, or vice-versa. Some groups may need to manually adjust gateways accordingly. In this regard, groups should particularly ensure that the Tasman, Drake, Tethys, and Panama gateways are all open, and that there is a connection between the Atlantic and the Arctic oceans. Note that the Tasman, Drake, and Arctic gateways are all relatively narrow and shallow, but are open in this reconstruction.

235 In addition to the absolute paleogeography, some climate models may require sub-gridscale topography to be prescribed, in particular for gravity-wave drag parameterisations. If this is the case, then modelling groups should implement subgridscale fields as they see fit. A typical approach previously used in Phase 1 is to correlate subgridscale parameters with absolute heights for the modern (outside of Antarctica), and then apply the resulting functions to the absolute Eocene topography to generate the required Eocene sub-gridscale fields. See Section 4.2.1 of Lunt et al. (2017) for more details. An alternative approach is



to calculate subgrid-scale topographies directly from the Eocene paleogeography, but care must be taken that resulting Eocene subgrid-scale topographies are consistent with those of the preindustrial simulation.

We leave it to individual groups to decide how best to implement any necessary field of river-runoff routing, as the format
240 and requirements for such a field are very model-specific. A typical approach is to derive the routing field from the paleogeographic reconstruction (sometimes after interpolation to the model resolution), for example by following the path of steepest descent from each gridcell, until the coast is reached. Of key importance is that the approach taken, and resulting routing field, is documented by each group. We also note that Herold et al. (2014) provided an Eocene runoff routing field in their Supplementary Information.

245 Diapycnal mixing in the interior of the ocean is primarily driven by internal tides. The magnitude and distribution of the strength of tidal mixing is related to ocean geometry, and would therefore have been different to modern in the Eocene ocean (Green and Huber, 2013). Models often use prescribed values for mixing parameters and mixing parameterisations, and Ladant et al. (2024) have shown that using Eocene-specific tidal mixing can influence ocean circulation, and could potentially be important for correctly representing associated biogeochemical processes. Groups wishing to implement Eocene-specific tidal
250 mixing in their simulations can use the energy dissipation field provided in the Supplementary Information of Herold et al. (2014), which was based on the work of Green and Huber (2013).

In order to facilitate future model-data comparisons, we provide the paleo locations of the sites in the DeepMIP-Eocene proxy database (Hollis et al., 2019; Inglis et al., 2020a) in the new reference frame as an Excel file on Zenodo Lunt (2025b).

2.2.3 Vegetation Boundary Conditions

255 The vegetation in DeepMIP-Eocene Phase 1 was that of Herold et al. (2014). This was produced by running the BIOME4 vegetation model (Kaplan et al., 2003) forced by a pre-DeepMIP Eocene CESM simulation, with the results expressed using the megabiome classification of Harrison and Prentice (2003) (Figure 4a).

For Phase 2, we make use of work of Brugger et al. (in prep), who ran the LPJ-GUESS vegetation model (Smith et al., 2014) forced by all of the DeepMIP-Eocene Phase 1 climate model simulations. To better represent Eocene vegetation, plant
260 functional types were adjusted in these simulations by adding shrub plant functional types based on Allen et al. (2020) and deactivating grass plant functional types. Qualitative comparison of these results with a proxy paleoflora dataset of the Eocene Thompson et al. (2025), indicates best agreement between the model simulations and data for vegetation associated with the CESM1.2 simulation at $6 \times \text{PI}$ over most of the globe (see Appendix, Figure A2(a)), but a best fit with vegetation associated with the GFDL simulation at $6 \times \text{PI}$ over Antarctica (see Appendix, Figure A2(b)). Therefore, we choose this hybrid
265 CESM1.2/GFDL-forced LPJ-GUESS vegetation distribution as the starting point for the boundary condition for DeepMIP-Eocene Phase 2.

To produce the final data-model hybrid vegetation boundary condition, we integrated the palaeobotanical data-based reconstruction published in Thompson et al. (2025) with the CESM1.2/GFDL-forced LPJ-GUESS model-based vegetation simulation (Brugger et al. (in prep)). Following the approach previously applied in the framework of PlioMIP (Salzmann et al., 270 2008), we adjusted data-model mismatches only for regions with sufficient data coverage. These adjustments include extending

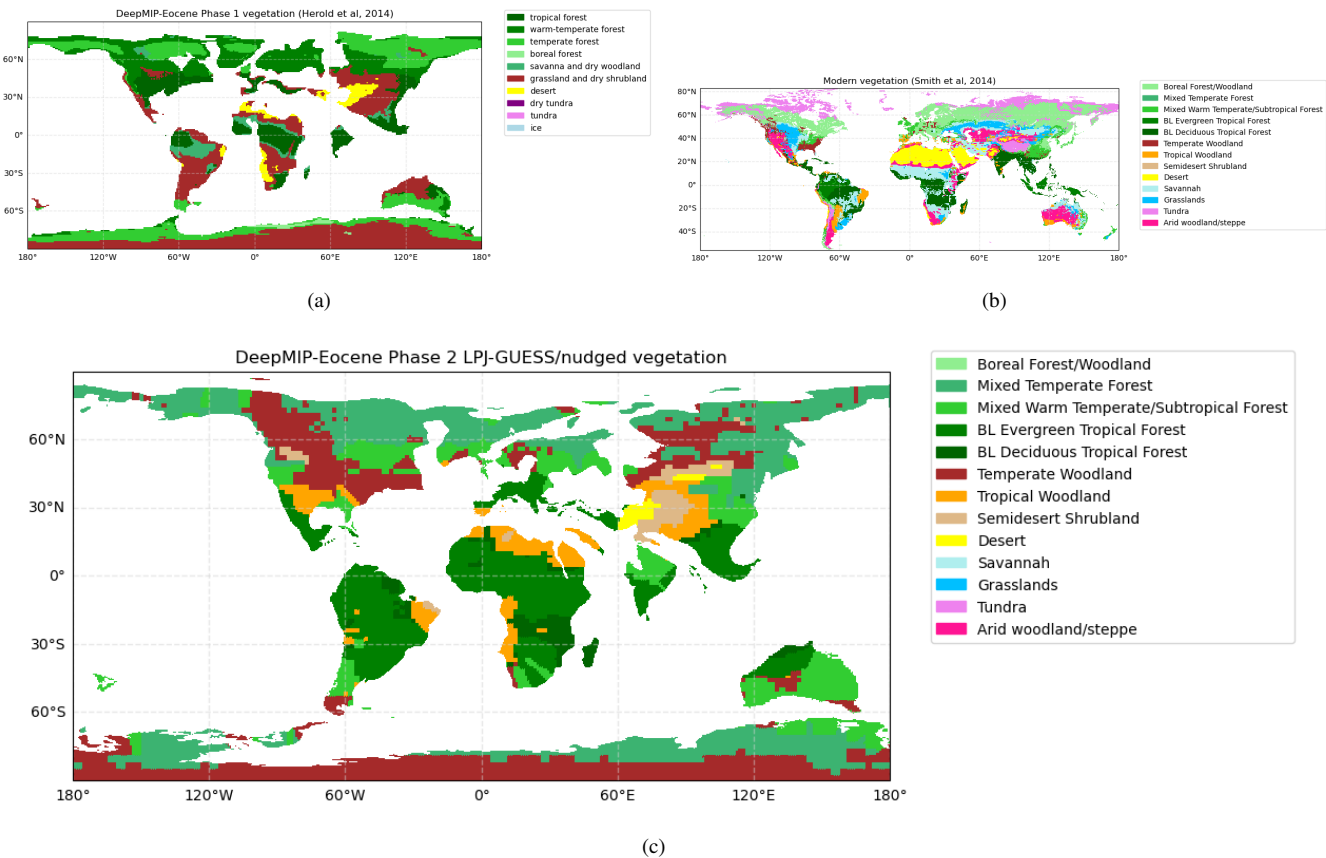


Figure 4. (a) The Herold et al. (2014) vegetation used in DeepMIP-Eocene Phase 1. (b) The modern vegetation of Smith et al. (2014), using LPJ-GUESS biomes. (c) DeepMIP-Eocene Phase 2 vegetation, which is derived from the LPJ-GUESS model when forced by the CESM1.2 and GFDL 6 \times PI simulations from Phase 1 of DeepMIP-Eocene, and nudged towards the vegetation proxy data of Thompson et al. (2025). Note that boreal forests, savannah, grasslands, and tundra vegetation types are not present in the Eocene LPJ-GUESS-based reconstruction in (c), but are included in the legend for comparison with the modern vegetation reconstruction in (a). Figure A2(c) in the Appendix shows the nudged vegetation in (c) prior to being regridded to the DeepMIP-Eocene Phase 2 reference frame and land-sea mask.

warm-temperate forest cover in East Asia, replacing boreal forest with temperate forests in West Siberia, and increasing the extent of dry woodlands in northern hemisphere subtropical regions (see Appendix, Figure A2(c)). This was then regridded to the new Phase 2 land-sea mask - the final result of this process is shown in Figure 4(c).

We note that the CO₂ of 6 \times PI in the underlying LPJ-GUESS vegetation model simulations is inconsistent with the 5 \times PI recommended in the DeepMIP-Eocene Phase 2 climate model simulations and based on CO₂ proxies. However, 5 \times PI simulations are not available from the last phase of DeepMIP-Eocene, and in any case, biases in the climate sensitivity of the climate models could result in an inconsistency between actual CO₂ and the CO₂ that results in the best fit to the vegetation data.



Similarly as for Phase 1, it is important that groups take care to implement this vegetation in a manner as consistent as possible with their preindustrial control simulation. This may mean converting the LPJ-GUESS vegetation types into the model's 280 intrinsic vegetation types, or converting the LPJ-GUESS vegetation types into land surface parameters such as albedo, roughness length etc. In either case, a modern map of vegetation, using the LPJ-GUESS vegetation types, is provided as a NetCDF file on Zenodo Lunt (2025b) to aid this process, and shown in Figure 4(b). Values of several land-surface parameters for typical vegetation types are available on the PRISM webpages: https://geology.er.usgs.gov/egpsc/prism/prism_1_23/ancillary/Biome-Megabiome_Lookup.html.

285 2.2.4 Other Boundary Conditions

The recommendation for all other boundary conditions remains unchanged from Phase 1. This includes soils and lakes (Section 4.2.2), non-CO₂ greenhouse gases (Section 4.2.3), aerosols (Section 4.2.4), and solar luminosity and astronomical (orbital) 290 parameters (Section 4.2.5); where the section numbers refer to Lunt et al. (2017), wherein detailed recommendations are given. In brief, soil parameters are globally homogeneous typical modern values, there are no lakes or ice sheets, non-CO₂ greenhouse gas concentrations are kept as preindustrial, several options are provided for aerosols, and solar luminosity and astronomical configurations are kept as modern. Due to the uncertainties in many of these aspects, suggested sensitivity studies are highlighted below.

2.3 Suggested sensitivity studies

Groups are encouraged to carry out any sensitivity studies that they are interested in, that best advance their scientific 295 understanding. Sometimes, it can be useful to have more than one group carry out a particular sensitivity study, to test model dependence. We therefore suggest some sensitivity studies that may be of particular interest, and provide NetCDF files on Zenodo Lunt (2025b) as appropriate. The names of the sensitivity simulations are summarised in Table 1.

2.3.1 Sensitivity studies to greenhouse gases and solar luminosity; simulations *deepmip-p2-sens-YxCO₂*, *deepmip-p2-sens-5xCO₂-solarmethane*, *equilibrium-4xCO₂*

300 As described in Section 2.1, one of the mandatory experiments in DeepMP Phase 2 is a sensitivity study with 1×PI, to identify the impact of CO₂ versus non-CO₂ forcings on Eocene climate (simulation *deepmip-p2-stand-1xCO₂*, see Table 1). In addition, we encourage EECO sensitivity studies at other CO₂ concentrations (simulations *deepmip-p2-sens-YxCO₂*, see Table 1), including 4×PI (also allowing comparison with an extended/equilibrated version of the CMIP *abrupt-4xCO₂* experiment; *equilibrium-4xCO₂*, see Table 1), 3×PI (also allowing comparison with the most common Eocene simulation from Phase 1), 305 and 6×PI (close to the top-end estimate of EECO CO₂ from Hönisch et al. (2023) and Rae et al. (2021)). These sensitivity simulations with various CO₂ levels could also be used to examine the potential nonlinearity in the sensitivity of Eocene temperatures to CO₂ (Zhu et al., 2019; Caballero and Huber, 2013). We also encourage abrupt CO₂ changes to estimate the



ECS of the Eocene configuration (in particular an abrupt quadrupling from $1\times\text{PI}$ to $4\times\text{PI}$ for comparison with the modern *abrupt-4xCO₂* experiment).

310 Given that there is evidence that there were more wetlands in the Eocene compared with modern (Wilton et al., 2019), and that there were perturbations to the CH₄ cycle during the PETM (Inglis et al., 2020b), it is probable that CH₄ concentrations during the EECO were higher than modern. For DeepMIP-Eocene Phase 1, Lunt et al. (2017) justified keeping non-CO₂ greenhouse gases as preindustrial and solar luminosity as modern, by arguing that their respective forcings broadly cancelled out. However, this neglects the substantial uncertainty in Eocene CH₄ (and other non-CO₂ greenhouse gas) forcing, and neglects 315 that even if these two forcings balance in the global annual mean, seasonal and spatial residuals in the climate response will still remain (Lunt et al., 2008). We therefore encourage sensitivity studies in which changes in solar luminosity and CH₄ are separately represented (simulation *deepmip-p2-sens-5xCO2-solarmethane*, see Table 1). For solar luminosity we recommend the value of 1355 W m⁻² for 51 Ma (Gough, 1981). For CH₄, a value of 3000 ppb for the early Eocene is consistent with the modelling work of Beerling et al. (2011). This was the value calculated in Lunt et al. (2017) to roughly cancel the solar 320 luminosity change, see their Section 4.2.3. However, Beerling et al. (2011) also quotes a range between 2580 - 3614 ppb, so other values may be preferred.

2.3.2 Sensitivity studies to paleogeography; simulation *deepmip-p2-sens-5xCO2-paleogeog*

Some groups may wish to explore the difference between the Phase 1 paleogeography of Herold et al. (2014) and the new Phase 2 paleogeography. We therefore provide the Herold et al. (2014) paleogeography on the new Phase 2 reference frame (at 325 55 Ma for consistency with the original Herold et al. (2014) reconstruction) as a NetCDF file on Zenodo Lunt (2025b), because the reference frame has been shown to influence atmospheric and ocean circulation (Baatsen et al., 2018; Zhang et al., 2024).

2.3.3 Sensitivity studies to vegetation and land surface parameters ; simulation *deepmip-p2-sens-5xCO2-thompson*

An alternative Phase 2 vegetation dataset is provided by Thompson et al. (2025). In this case, a similar approach is taken as in Brugger et al. (in prep), but the BIOME4 vegetation model (Kaplan et al., 2003) is used in place of the LPJ-GUESS 330 model. Thompson et al. (2025) find that the vegetation associated with the CESM1.2 and GFDL_CM2.1 models at $6\times\text{PI}$ best fit the vegetation proxy data. Given that the CESM1.2 model (Hurrell et al., 2013) runs at a higher horizontal and vertical resolution than the GFDL_CM2.1 model (Delworth et al., 2006) and was developed more recently, and is therefore likely to overall have a more accurate representation of physical processes, we use the CESM1.2-based vegetation as the main sensitivity 335 study in DeepMIP-Eocene Phase 2. Again, we note that this CO₂ concentration is inconsistent with the $5\times\text{PI}$ recommended in the DeepMIP-Eocene Phase 2 climate model simulations. We encourage groups to carry out sensitivity studies using this Thompson et al. (2025) vegetation, which is shown in Figure 5. However, in contrast to our LPJ-GUESS model and proxy hybrid reconstruction, this BIOME4 vegetation shows widespread discrepancies in the subtropics and mid-latitudes between proxy-reconstructed forests and woodlands and modelled dry shrublands and deserts (Thompson et al., 2025). Similarly as for the LPJ-GUESS vegetation, a modern vegetation map using the BIOME4 vegetation types is provided (Figure 5(b), see Section 340 4.2.2 of Lunt et al. (2017) for more details).

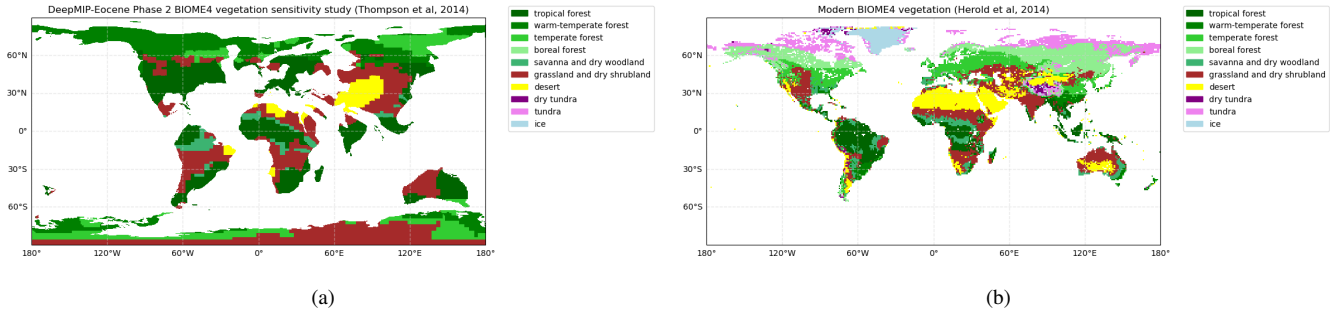


Figure 5. (a) The Thompson et al. (2025) vegetation, suggested as a sensitivity study in DeepMIP-Eocene Phase 2, which is the output of the BIOME4 model when forced by the CESM1.2 $6\times\text{PI}$ simulations from Phase 1 of DeepMIP. For comparison with the standard DeepMIP-Eocene Phase 2 vegetation in Figure 4c. (b) Modern vegetation using the same biome classification as BIOME4 (Herold et al., 2014)

Furthermore, we encourage sensitivity studies to lake distributions, as these have been shown to be potentially important for determining Eocene hydrology and climate, through changes in surface heat capacity and formation of low clouds (Henry and Vallis, 2022). Similarly, modified Eocene soil characteristics are likely to play a role, given their impact on warm climate simulations of the Pliocene (Pound et al., 2014). Although there are global maps of soils and lakes for the Pliocene based on 345 proxy data (Pound et al., 2014), no such global datasets exist for the early Eocene as far as we are aware. As such, Eocene sensitivity studies are likely to be somewhat idealised, but could be modified in association with the vegetation types, as is defined for DeepMIP-Miocene (Bradshaw et al., 2025).

2.3.4 Other sensitivity studies

As in Phase 1, we also encourage sensitivity studies to astronomical (orbital) parameters (see Ross (2023) and Section 4.3.3 350 in Lunt et al. (2017)), and to initialisation (Section 4.3.7 in Lunt et al., 2017). Other aspects that groups may wish to explore include aerosols (Kiehl and Shields, 2013), atmospheric chemistry, including for example methane-ozone-hydroxyl interactions (Beerling et al., 2011), model resolution (Nooteboom et al., 2022), dynamic vegetation (Loptson et al., 2014), tidal mixing (Ladant et al., 2024), stable water isotopes (Zhu et al., 2020), and internal model parameters (Sagoo et al., 2013). Groups may 355 also wish to carry out high-resolution atmosphere-only simulations to explore processes/features such as atmospheric rivers (Shields et al., 2021).

2.4 Initial conditions, integration length, and assessment of equilibrium

In Phase 1, a recommendation was given for oceanic temperature and salinity initial conditions. This was a linear decrease of 360 temperature with depth, as a function of latitude, and a globally constant salinity of 34.7 psu (see Equation 1 in Lunt et al., 2017). However, several groups found that the model became unstable with this initial condition, and other groups found that it resulted in very long spinup times, as the linear decrease with depth resulted in an excess of energy at intermediate depths



which took a long time to dissipate. As such, in Phase 2 we are less prescriptive, and encourage groups to use their preferred method for initialisation. As an example, groups may choose to initialise from spun-up oceanic states from previous Phase 1 simulations, carried out with their own or other models, and available in the DeepMIP-Eocene Phase 1 model database (Steinig et al., 2024). In this case, we encourage groups to use appropriate initial conditions according to the CO₂ concentration at 365 which they are running (see discussion in Steinig et al., in prep), and accounting for the climate sensitivity of their model. In addition, we suggest that groups initialise with relatively warm temperatures in the deep ocean, because doing so may potentially accelerate spin-up by enabling the activation of a meridional overturning circulation more quickly, as opposed to remaining stratified for a relatively long time due to a ‘cold-start’. Alternatively, groups may wish to use ocean proxy data to inform the initialisation of the temperature and salinity fields. In any case, we strongly recommend that groups initialise 370 temperature and salinity in a mutually consistent fashion, to avoid spurious density contrasts early in the simulation.

As in Phase 1, simulations should be carried out for as long as possible, in order to reach as close to equilibrium as possible. In Phase 1, a mean absolute TOA imbalance of less than 0.3 W m⁻² was required. Since then, de Boer et al. (in press) have shown that substantial climatological and ocean circulation changes can take place following additional spinup after a threshold of 0.3 W m⁻² has been reached. Therefore, in Phase 2 we strongly encourage groups to aim for a mean absolute TOA imbalance 375 over the final 100 years of the simulations (i.e. the period uploaded to the DeepMIP database) of less than 0.1 W m⁻² and deep ocean temperature (at 3500 m) trends of less than 0.1 °/century. For those models for which the TOA energy budget is not closed, the TOA imbalance should be similar to that of an equilibrated preindustrial control simulation. These reduced thresholds particularly apply to the ‘standard’ simulations (*deepmip-p2-stand-5xCO2* and *deepmip-p2-stand-1xCO2*; see Table 1). We encourage groups to report their extrapolated full-equilibrium temperature as derived from a ‘Gregory plot’ (Gregory 380 et al., 2004). Given that these thresholds are not necessarily sufficient to indicate an ocean circulation in quasi-equilibrium, modelling groups are encouraged to report time series of key ocean variables to enable diagnoses of ocean equilibrium (de Boer et al., in press) (See Section 2.5). Groups may also choose to carry out ‘ocean surgery’ during a simulation (Steinig et al., in prep), in which instantaneous perturbations are applied to the ocean temperature field in an attempt to accelerate the progression towards full equilibrium.

385 2.5 Model outputs

We strongly encourage groups to upload their simulation boundary conditions and outputs to the DeepMIP database (Steinig et al., 2024). Instructions for uploading data are given here: <https://www.deepmip.org/data>. We encourage groups to provide means and standard deviations of the last 100 years of their simulations for multiple variables, and timeseries of the last 100 years of their simulations for selected variables. Each output variable is stored in a separate file according to the following 390 structure:

```
directory = deepmip-eocene-p2/<Family>/<Model>/<Experiment>/<Version>/<Averaging>  
filename = <Variable>_<Model>_<Experiment>_<Version>.<Statistic>.nc  
where:
```



395 – <Family> and <Model> describe the model used to carry out the simulations (see Table 1 in Steinig et al., 2024, for examples from Phase 1).

400 – <Experiment> is listed Table 1 of this paper (also see Table 2 in Steinig et al., 2024, for examples from Phase 1).

405 – <Variable> represents the variable name; we encourage all groups to use CF-compliant (Eaton et al., 2023) variable names. A list of commonly-used variables from Phase 1 is given in Tables 4 (atmosphere) and 5 (ocean) of Steinig et al. (2024); in addition, studies of ocean mixing would benefit from the total vertical diffusivity coefficient (and its contributions, if relevant), the Brunt-Väisälä frequency, and the power consumed by mixing processes.

– <Statistic> is either ‘mean’ (1 or 12 timesteps for annual or monthly means), ‘std’ (1 or 12 timesteps for annual or monthly means), ‘time_series’ (1200 timesteps) or omitted for the time-independent boundary conditions.

– <Averaging> can either be ‘climatology’ or ‘time_series’. ‘Climatology’ denotes the directory for storing the (smaller) climatological mean and standard deviation (‘mean’ and ‘std’ files). ‘time_series’ denotes the directory for storing the (larger) ‘time_series’ files to enable more granular download options.

We further strongly encourage modelling groups to upload full simulation-length time series of key oceanic variables to diagnose the equilibrium state of the ocean. These are the mean temperature at 3500 m, and where available also the mean ocean ideal age tracer at this depth. We further encourage the reporting of key meridional overturning circulation (MOC) streamfunction maxima and minima, and suggest specifically the outputs: Atlantic MOC: maximum between 45°N-68°N; 410 Pacific MOC: maximum between 25°N-58°N; Global GMOC: maximum global MOC north of 40°S; Southern Ocean MOC: absolute of minimum of the GMOC south of 60°S. All metrics should be calculated below 500 m depth to exclude the wind-driven gyres (de Boer et al., in press).

For those models with an irregular ocean (and/or atmospheric) grid, in addition to the native grid, the results should also be interpolated to a regular lat-lon grid prior to uploading to the database. In this case, care should be taken that the global mean 415 of relevant variables is conserved.

3 Summary and Plans for analysis

We have provided a framework for groups to carry out consistent sets of climate model simulations of the early Eocene, facilitating model-data comparisons and exploration of sensitivities. We hope that modelling groups will soon begin to start simulations within this new framework, and have a ‘stretch goal’ to have some simulations available in time for inclusion 420 in IPCC AR7. In any case, we anticipate, as was the case for Phase 1, that this framework will lead on to multiple studies exploring multiple aspects of the Earth system under a high-CO₂ warm climate. Again, as in Phase 1, we anticipate that those scientists who carry out the model simulations will be able to actively contribute to many of these papers, bringing their own expertise about their models to the analysis, and recognising their hard work in configuring and carrying out their simulations.



We also anticipate that the DeepMIP proxy database will be expanded and developed over this period, leading to new insights
425 and more robust model-data comparisons.

Code and data availability. The current version of the code associated with this paper is available from the project website <https://github.com/danlunt1976/DeepMIP-Eocene-p2> under the GNU General Public License version 3. The exact version of the code and files associated with this paper are archived on Zenodo under DOI 10.5281/zenodo.17887456 and 10.5281/zenodo.17899194 respectively (Lunt, 2025a, b).

Appendix A

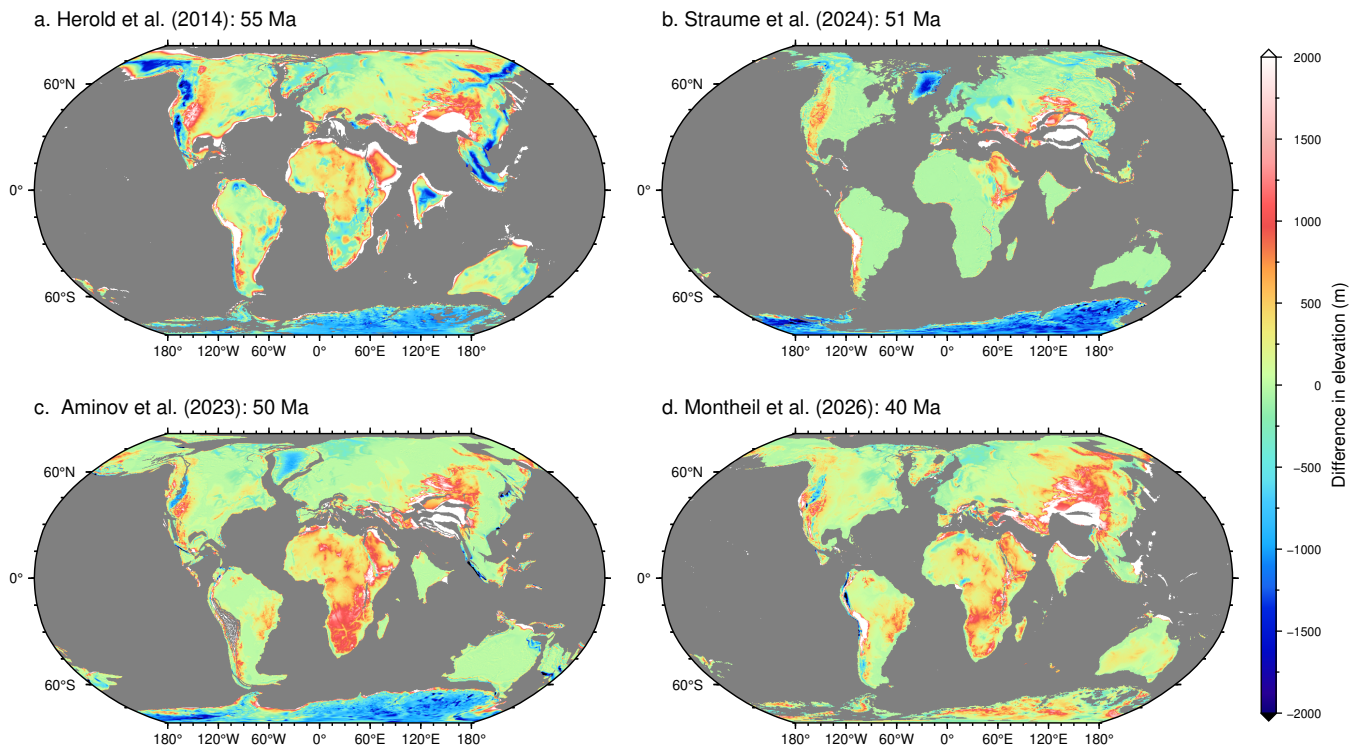


Figure A1. Difference in height between the four Eocene paleogeographies considered in this paper and the modern ETOPO5 geography (National Geophysical Data Center, 1993), with the modern geography rotated to the appropriate Eocene time period for each paleogeography.

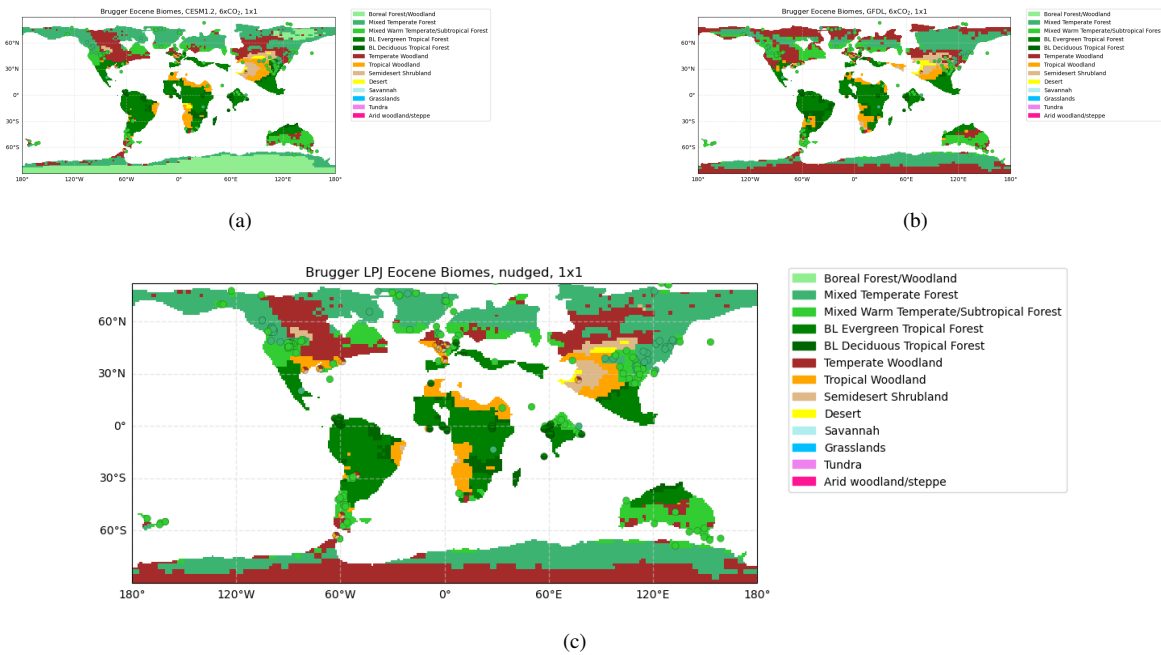


Figure A2. (a) The original vegetation from Brugger et al. (in prep), with LPJ-GUESS forced by the DeepMIP Phase 1 simulations from (a) CESM1.2 at $6\times\text{PI}$ and (b) GFDL at $6\times\text{PI}$. (c) The hybrid proxy-model reconstruction, which is then regridded to the DeepMIP Phase 2 reference frame, as shown in the main paper in Figure 3c. Superimposed on all plots is the vegetation proxy data of Thompson et al. (2025).

430 *Author contributions.* DJL conceived the paper and wrote the first draft. NMW produced the new DeepMIP-Eocene Phase 2 paleogeography boundary conditions, with input from BV. JB, US, and DH produced the new DeepMIP-Eocene Phase 2 vegetation boundary conditions, with input from TH. JWBR provided input to the CO_2 reconstruction. All authors contributed to the writing of the paper.

Competing interests. The authors declare no competing interests.

435 *Acknowledgements.* DJL thanks NERC grant SWEET (NE/P01903X/1), NERC grant DeepMIP (NE/N006828/1), NERC grant PaleoGrad-
 Phan (NE/X000222/1), and EU grant Past2Future (Grant Agreement 101184070). DJL also acknowledges support provided through an
 NCAR affiliate scientist appointment. DKH acknowledges support from Australian Research Council grant DE220100279. US acknowledges
 NERC grant NE/P019137/1. GNI was supported by a Royal Society Dorothy Hodgkin Fellowship (DHF/R1\191178). JZ acknowledges
 support from the National Science Foundation grant no. 2202777 and 2303567 and Heising-Simons Foundation grant no. 2023-4716. The
 CESM project is supported primarily by the U.S. National Science Foundation (NSF). This material is based upon work supported by the
 440 NSF National Center for Atmospheric Research, which is a major facility sponsored by the NSF under Cooperative Agreement No. 1852977.
 R. P. Acosta and N. J. Burls acknowledge support from NSF EAR-2303417. AS acknowledges the Netherlands Organization for Scientific



Research grant SUMMIT.1.034 - EMBRACER. JAMG acknowledges support from NERC through MATCH (NE/S009566/1). AdB acknowledges support from Swedish Research Council grant 2020-04791. NMW acknowledges support from the Australian Research Council grant IE230100098. DRG acknowledges support from Natural Sciences and Engineering Research Council (Canada) Discovery grant RGPIN-445 2016-04337. JWBR acknowledges funding from the European Research Council under the European Union's Horizon 2020 research and innovation program (grant agreement 805246). DE acknowledges support from the Royal Society (award reference URF\R1\221735) and UKRI (UKRI Frontier Research Guarantee Proposal (Horizon Europe ERC Starting Grants Guarantee), award reference EP/Y034252/1).



References

Abhik, S., Capitanio, F., Dommenget, D., Goswami, B., Farnsworth, A., Hutchinson, D., Arblaster, J., Lunt, D., and Steinig, S.: 450 Unraveling weak and short South Asian wet season in the Early Eocene warmth, *Communications Earth and Environment*, 5, <https://doi.org/10.1038/s43247-024-01289-8>, 2024.

Allen, J. R. M., Forrest, M., Hickler, T., Singarayer, J. S., Valdes, P. J., and Huntley, B.: Global vegetation patterns of the past 140,000 years, *Journal of Biogeography*, 47, 2073–2090, [https://doi.org/https://doi.org/10.1111/jbi.13930](https://doi.org/10.1111/jbi.13930), 2020.

Aminov, J., Dupont-Nivet, G., Ruiz, D., and Gailleton, B.: Paleogeographic reconstructions using QGIS: Introducing Terra Antiqua plugin and its application to 30 and 50 Ma maps, *Earth-Science Reviews*, 240, 104401, <https://doi.org/https://doi.org/10.1016/j.earscirev.2023.104401>, 2023.

Anagnostou, E., John, E. H., Edgar, K. M., Foster, G. L., Ridgwell, A., Inglis, G. N., Pancost, R. D., Lunt, D. J., and Pearson, P. N.: Changing atmospheric co₂ concentration was the primary driver of early cenozoic climate, *Nature*, 533, 380–384, <https://doi.org/10.1038/nature17423>, 2016.

Anagnostou, E., John, E., Babilia, T., Sexton, P., Ridgwell, A., Lunt, D., Pearson, P., Chalk, T., Pancost, R., and Foster, G.: Proxy evidence 460 for state-dependence of climate sensitivity in the Eocene greenhouse, *Nature Communications*, 11, <https://doi.org/10.1038/s41467-020-17887-x>, 2020.

Arias, P. A., Bellouin, N., Coppola, E., Jones, R. G., Krinner, G., Marotzke, J., Naik, V., Palmer, M. D., Plattner, G.-K., Rogelj, J., Rojas, M., Sillmann, J., Storelvmo, T., Thorne, P. W., Trewin, B., Achuta Rao, K., Adhikary, B., Allan, R. P., Armour, K., Bala, G., Barimalala, 465 R., Berger, S., Canadell, J. G., Cassou, C., Cherchi, A., Collins, W., Collins, W. D., Connors, S. L., Corti, S., Cruz, F., Dentener, F. J., Dereczynski, C., Di Luca, A., Diongue Niang, A., Doblas-Reyes, F. J., Dosio, A., Douville, H., Engelbrecht, F., Eyring, V., Fischer, E., Forster, P., Fox-Kemper, B., Fuglestvedt, J. S., Fyfe, J. C., Gillett, N. P., Goldfarb, L., Gorodetskaya, I., Gutierrez, J. M., Hamdi, R., Hawkins, E., Hewitt, H. T., Hope, P., Islam, A. S., Jones, C., Kaufman, D. S., Kopp, R. E., Kosaka, Y., Kossin, J., Kravovska, S., Lee, J.-Y., Li, J., Mauritzen, T., Maycock, T. K., Meinshausen, M., Min, S.-K., Monteiro, P. M. S., Ngo-Duc, T., Otto, F., Pinto, I., 470 Pirani, A., Raghavan, K., Ranasinghe, R., Ruane, A. C., Ruiz, L., Sallée, J.-B., Samset, B. H., Sathyendranath, S., Seneviratne, S. I., Sörensson, A. A., Szopa, S., Takayabu, I., Treguier, A.-M., van den Hurk, B., Vautard, R., von Schuckmann, K., Zaehle, S., Zhang, X., and Zickfeld, K.: Technical Summary, in: *Climate Change 2021: The Physical Science Basis. Contribution of Working Group I to the Sixth Assessment Report of the Intergovernmental Panel on Climate Change*, edited by Masson-Delmotte, V., Zhai, P., Pirani, A., Connors, S. L., Péan, C., Berger, S., Caud, N., Chen, Y., Goldfarb, L., Gomis, M. I., Huang, M., Leitzell, K., Lonnoy, E., Matthews, J. B. R., Maycock, T. K., Waterfield, T., Yelekçi, O., Yu, R., and Zhou, B., Cambridge University Press, Cambridge, UK and New York, NY, USA, <https://doi.org/10.1017/9781009157896.002>, 2021.

Baatsen, M., von der Heydt, A., Kliphuis, M., Viebahn, J., and Dijkstra, H.: Multiple states in the late Eocene ocean circulation, *Global and Planetary Change*, 163, 18–28, <https://doi.org/https://doi.org/10.1016/j.gloplacha.2018.02.009>, 2018.

Beerling, D., Fox, A., Stevenson, D., and Valdes, P.: Enhanced chemistry-climate feedbacks in past greenhouse worlds, *Proceedings of the 480 National Academy of Sciences (PNAS)*, 108, 9770–9775, <https://doi.org/10.1073/pnas.1102409108>, 2011.

Boschman, L. M.: Andean mountain building since the Late Cretaceous: A paleoelevation reconstruction, *Earth-Science Reviews*, 220, 103 640, <https://doi.org/https://doi.org/10.1016/j.earscirev.2021.103640>, 2021.

Bradshaw, C., Fletcher, T., Reichgelt, T., Akgün, F., Cantrill, D. J., Casas-Gallego, M., Doláková, N., Erdei, B., Kayseri-Özer, M. S., Kováčová, M., Ochoa, D., Pound, M., Utescher, T., Zhao, J., Sepulchre, P., Feakins, S. J., Ivanov, D., Li, S., Miao, Y., Worobiec, E.,



485 Strömberg, C. A., Novak, J., Herold, N., Huber, M., Frigola, A., Prange, M., Knorr, G., Lohmann, G., Farnsworth, A., Li, Y., Lunt, D. J., Pillot, Q., Donnadieu, Y., Acosta, R. P., and Burls, N.: MioVeg1: A Global Middle Miocene Vegetation Reconstruction for Climate Modeling, *Paleoceanography and Paleoclimatology*, 40, [https://doi.org/https://doi.org/10.1029/2025PA005213](https://doi.org/10.1029/2025PA005213), 2025.

Brinkhuis, H., Schouten, S., Collinson, M. E., Sluijs, A., Damsté, J. S. S., Dickens, G. R., Huber, M., Cronin, T. M., Onodera, J., Takahashi, K., Bujak, J. P., Stein, R., van der Burgh, J., Eldrett, J. S., Harding, I. C., Lotter, A. F., Sangiorgi, F., van Konijnenburg-van Cittert, H., de Leeuw, J. W., Matthiessen, J., Backman, J., Moran, K., Clemens, S., Eynaud, F., Gattaccea, J., Jakobsson, M., Jordan, R., Kaminski, M., King, J., Koc, N., Martinez, N. C., McInroy, D., Moore, T. C. J., O'Regan, M., Pälike, H., Rea, B., Rio, D., Sakamoto, T., Smith, D. C., StJohn, K. E. K., Suto, I., Suzuki, N., Watanabe, M., and Yamamoto, M.: Letter. Episodic fresh surface waters in the Eocene Arctic Ocean, *Nature*, 441, 606–609, 2006.

490 Brugger, J., Thompson, N., Utescher, T., Salzmann, U., and Hickler, T.: Simulating the terrestrial biosphere in the high CO₂ world of the early Eocene, -, -, -, in prep.

Burke, K., Williams, J., Chandler, M., Haywood, A., Lunt, D., and Otto-Bliesner, B.: Pliocene and Eocene provide best analogs for near-future climates, *Proceedings of the National Academy of Sciences of the United States of America*, 115, 13 288–13 293, <https://doi.org/10.1073/pnas.1809600115>, 2018.

Burls, N. J., Bradshaw, C. D., De Boer, A. M., Herold, N., Huber, M., Pound, M., Donnadieu, Y., Farnsworth, A., Frigola, A., 500 Gasson, E., von der Heydt, A. S., Hutchinson, D. K., Knorr, G., Lawrence, K. T., Lear, C. H., Li, X., Lohmann, G., Lunt, D. J., Marzocchi, A., Prange, M., Riihimaki, C. A., Sarr, A.-C., Siler, N., and Zhang, Z.: Simulating Miocene Warmth: Insights From an Opportunistic Multi-Model Ensemble (MioMIP1), *Paleoceanography and Paleoclimatology*, 36, e2020PA004054, <https://doi.org/https://doi.org/10.1029/2020PA004054>, e2020PA004054 2020PA004054, 2021.

Caballero, R. and Huber, M.: State-dependent climate sensitivity in past warm climates and its implications for future climate projections, 505 *Proceedings of the National Academy of Sciences*, 110, 14 162–14 167, 2013.

Couvreur, T. L., Dauby, G., Blach-Overgaard, A., Deblauwe, V., Dessein, S., Droissart, V., Hardy, O. J., Harris, D. J., Janssens, S. B., Ley, A. C., Mackinder, B. A., Sonké, B., Sosef, M. S., Stévert, T., Svenning, J.-C., Wieringa, J. J., Faye, A., Missoup, A. D., Tolley, K. A., Nicolas, V., Ntie, S., Fluteau, F., Robin, C., Guillocheau, F., Barboni, D., and Sepulchre, P.: Tectonics, climate and the diversification of the tropical African terrestrial flora and fauna, *Biological Reviews*, 96, 16–51, <https://doi.org/https://doi.org/10.1111/brv.12644>, 2021.

510 Cramwinckel, M., Burls, N., Fahad, A., Knapp, S., West, C., Reichgelt, T., Greenwood, D., Chan, W., Donnadieu, Y., Hutchinson, D., de Boer, A., Ladant, J., Morozova, P., Niegzodzki, I., Knorr, G., Steinig, S., Zhang, Z., Zhu, J., Feng, R., Lunt, D., Abe-Ouchi, A., and Inglis, G.: Global and Zonal-Mean Hydrological Response to Early Eocene Warmth, *Paleoceanography and Paleoclimatology*, 38, <https://doi.org/10.1029/2022PA004542>, 2023.

de Boer, A. M., Krishnan, S., Burls, N. J., Hutchinson, D. K., and Renoult, M.: Evaluation of Quasi-equilibrium Criteria for Coupled Climate 515 1 Model Simulations, *Geophysical Research Letters*, -, -, in press.

Delworth, T. L., Broccoli, A. J., Rosati, A., Stouffer, R. J., Balaji, V., Beesley, J. A., Cooke, W. F., Dixon, K. W., Dunne, J., Dunne, K. A., Durachta, J. W., Findell, K. L., Ginoux, P., Gnanadesikan, A., Gordon, C. T., Griffies, S. M., Gudgel, R., Harrison, M. J., Held, I. M., Hemler, R. S., Horowitz, L. W., Klein, S. A., Knutson, T. R., Kushner, P. J., Langenhorst, A. R., Lee, H.-C., Lin, S.-J., Lu, J., Malyshev, S. L., Milly, P. C. D., Ramaswamy, V., Russell, J., Schwarzkopf, M. D., Shevliakova, E., Sirutis, J. J., Spelman, M. J., Stern, W. F., Winton, M., Wittenberg, A. T., Wyman, B., Zeng, F., and Zhang, R.: GFDL's CM2 Global Coupled Climate Models. Part I: Formulation and Simulation Characteristics, *Journal of Climate*, 19, 643–674, <https://doi.org/10.1175/JCLI3629.1>, 2006.



Dunne, J. P., Hewitt, H. T., Arblaster, J. M., Bonou, F., Boucher, O., Cavazos, T., Dingley, B., Durack, P. J., Hassler, B., Juckes, M., Miyakawa, T., Mzielinski, M., Naik, V., Nicholls, Z., O'Rourke, E., Pincus, R., Sanderson, B. M., Simpson, I. R., and Taylor, K. E.: An evolving Coupled Model Intercomparison Project phase 7 (CMIP7) and Fast Track in support of future climate assessment, *Geoscientific Model Development*, 18, 6671–6700, <https://doi.org/10.5194/gmd-18-6671-2025>, 2025.

Eaton, B., Gregory, J., Drach, B., Taylor, K., Hankin, S., Caron, J., Signell, R., Bentley, P., Rappa, G., Höck, H., Pamment, A., Juckes, M., Raspaud, M., Blower, J., Horne, R., Whiteaker, T., Blodgett, D., Zender, C., Lee, D., Hassell, D., Snow, A. D., Kölling, T., Allured, D., Jelenak, A., Soerensen, A. M., Gaultier, L., Herlédan, S., Manzano, F., Bärring, L., Barker, C., and Bartholomew, S. L.: NetCDF Climate and Forecast (CF) Metadata Conventions, <https://doi.org/10.5281/zenodo.14275572>, 2023.

Evans, D., Brugger, J., Inglis, G. N., and Valdes, P.: The Temperature of the Deep Ocean Is a Robust Proxy for Global Mean Surface Temperature During the Cenozoic, *Paleoceanography and Paleoclimatology*, 39, e2023PA004788, <https://doi.org/https://doi.org/10.1029/2023PA004788>, e2023PA004788, 2024.

Forster, P., Storelvmo, T., Armour, K., Collins, W., Dufresne, J.-L., Frame, D., Lunt, D., Mauritzen, T., Palmer, M., Watanabe, M., Wild, M., and Zhang, H.: The Earth's Energy Budget, Climate Feedbacks, and Climate Sensitivity, in: *Climate Change 2021: The Physical Science Basis. Contribution of Working Group I to the Sixth Assessment Report of the Intergovernmental Panel on Climate Change*, edited by Masson-Delmotte, V., Zhai, P., Pirani, A., Connors, S., Péan, C., Berger, S., Caud, N., Chen, Y., Goldfarb, L., Gomis, M., Huang, M., Leitzell, K., Lonnoy, E., Matthews, J., Maycock, T., Waterfield, T., Yelekçi, O., Yu, R., and Zhou, B., p. 923–1054, Cambridge University Press, Cambridge, United Kingdom and New York, NY, USA, <https://doi.org/10.1017/9781009157896.009>, 2021.

Goudsmit-Harzevoort, B., Lansu, A., Baatsen, M. L. J., von der Heydt, A. S., de Winter, N. J., Zhang, Y., Abe-Ouchi, A., de Boer, A., Chan, W.-L., Donnadieu, Y., Hutchinson, D. K., Knorr, G., Ladant, J.-B., Morozova, P., Niezgodzki, I., Steinig, S., Tripati, A., Zhang, Z., Zhu, J., and Ziegler, M.: The Relationship Between the Global Mean Deep-Sea and Surface Temperature During the Early Eocene, *Paleoceanography and Paleoclimatology*, 38, e2022PA004532, <https://doi.org/https://doi.org/10.1029/2022PA004532>, e2022PA004532, 2022PA004532, 2023.

Gough, D.: Solar interior structure and luminosity variations, *Solar Physics*, 74, 21–34, 1981.

Green, J. A. M. and Huber, M.: Tidal dissipation in the early Eocene and implications for ocean mixing, *Geophysical Research Letters*, 40, 2707–2713, <https://doi.org/https://doi.org/10.1002/grl.50510>, 2013.

Gregory, J. M., Ingram, W. J., Palmer, M. A., Jones, G. S., Stott, P. A., Thorpe, R. B., Lowe, J. A., Johns, T. C., and Williams, K. D.: A new method for diagnosing radiative forcing and climate sensitivity, *Geophysical Research Letters*, 31, <https://doi.org/https://doi.org/10.1029/2003GL018747>, 2004.

Harrison, S. P. and Prentice, C. I.: Climate and CO₂ controls on global vegetation distribution at the last glacial maximum: analysis based on palaeovegetation data, biome modelling and palaeoclimate simulations, *Global Change Biology*, 9, 983–1004, <https://doi.org/https://doi.org/10.1046/j.1365-2486.2003.00640.x>, 2003.

Haywood, A., Tindall, J., Burton, L., Chandler, M., Dolan, A., Dowsett, H., Feng, R., Fletcher, T., Foley, K., Hill, D., Hunter, S., Otto-Bliesner, B., Lunt, D., Robinson, M., and Salzmann, U.: Pliocene Model Intercomparison Project Phase 3 (PlioMIP3) – Science plan and experimental design, *Global and Planetary Change*, 232, 104316, <https://doi.org/https://doi.org/10.1016/j.gloplacha.2023.104316>, 2024.

He, Z., Zhang, Z., and Guo, Z.: Reconstructing early Eocene (~55 Ma) paleogeographic boundary conditions for use in paleoclimate modelling, *Science China Earth Sciences*, 62, 1416–1427, <https://doi.org/10.1007/s11430-019-9366-2>, 2019.

Henry, M. and Vallis, G. K.: Variations on a Pathway to an Early Eocene Climate, *Paleoceanography and Paleoclimatology*, 37, e2021PA004375, <https://doi.org/https://doi.org/10.1029/2021PA004375>, e2021PA004375, 2022PA004375, 2022.



560 560 Herold, N., Buzan, J., Seton, M., Goldner, A., Green, J. A. M., Müller, R. D., Markwick, P., and Huber, M.: A suite of early Eocene (55 Ma) climate model boundary conditions, *Geoscientific Model Development*, 7, 2077–2090, <https://doi.org/10.5194/gmd-7-2077-2014>, 2014.

Hollis, C. J., Dunkley Jones, T., Anagnostou, E., Bijl, P. K., Cramwinckel, M. J., Cui, Y., Dickens, G. R., Edgar, K. M., Eley, Y., Evans, D., Foster, G. L., Frieling, J., Inglis, G. N., Kennedy, E. M., Kozdon, R., Lauretano, V., Lear, C. H., Littler, K., Lourens, L., Meckler, A. N., Naafs, B. D. A., Pälike, H., Pancost, R. D., Pearson, P. N., Röhl, U., Royer, D. L., Salzmann, U., Schubert, B. A., Seebeck, H., Sluijs, A., Speijer, R. P., Stassen, P., Tierney, J., Tripati, A., Wade, B., Westerhold, T., Witkowski, C., Zachos, J. C., Zhang, Y. G., Huber, M., and Lunt, D. J.: The DeepMIP contribution to PMIP4: methodologies for selection, compilation and analysis of latest Paleocene and early Eocene climate proxy data, incorporating version 0.1 of the DeepMIP database, *Geoscientific Model Development*, 12, 3149–3206, <https://doi.org/10.5194/gmd-12-3149-2019>, 2019.

570 570 Hurrell, J. W., Holland, M. M., Gent, P. R., Ghan, S., Kay, J. E., Kushner, P. J., Lamarque, J. F., Large, W. G., Lawrence, D., Lindsay, K., Lipscomb, W. H., Long, M. C., Mahowald, N., Marsh, D. R., Neale, R. B., Rasch, P., Vavrus, S., Vertenstein, M., Bader, D., Collins, W. D., Hack, J. J., Kiehl, J. T., and Marshall, S.: The community earth system model: A framework for collaborative research, *Bulletin of the American Meteorological Society*, 94, 1339–1360, <https://doi.org/10.1175/BAMS-D-12-00121.1>, 2013.

Hönisch, B., Royer, D. L., Breecker, D. O., Polissar, P. J., Bowen, G. J., Henehan, M. J., Cui, Y., Steinthorsdottir, M., McElwain, J. C., Kohn, M. J., Pearson, A., Phelps, S. R., Uno, K. T., Ridgwell, A., Anagnostou, E., Austermann, J., Badger, M. P. S., Barclay, R. S., Bijl, P. K., Chalk, T. B., Scotese, C. R., de la Vega, E., DeConto, R. M., Dyez, K. A., Ferrini, V., Franks, P. J., Giulivi, C. F., Gutjahr, M., Harper, D. T., Haynes, L. L., Huber, M., Snell, K. E., Keisling, B. A., Konrad, W., Lowenstein, T. K., Malinverno, A., Guillermic, M., Mejía, L. M., Milligan, J. N., Morton, J. J., Nordt, L., Whiteford, R., Roth-Nebelsick, A., Rugenstein, J. K. C., Schaller, M. F., Sheldon, N. D., Sosdian, S., Wilkes, E. B., Witkowski, C. R., Zhang, Y. G., Anderson, L., Beerling, D. J., Bolton, C., Cerling, T. E., Cotton, J. M., Da, J., Ekart, D. D., Foster, G. L., Greenwood, D. R., Hyland, E. G., Jagniecki, E. A., Jasper, J. P., Kowalczyk, J. B., Kunzmann, L., Kürschner, W. M., Lawrence, C. E., Lear, C. H., Martínez-Botí, M. A., Maxbauer, D. P., Montagna, P., Naafs, B. D. A., Rae, J. W. B., Raitzsch, M., Retallack, G. J., Ring, S. J., Seki, O., Sepúlveda, J., Sinha, A., Tesfamichael, T. F., Tripati, A., van der Burgh, J., Yu, J., Zachos, J. C., and Zhang, L.: Toward a Cenozoic history of atmospheric CO₂, *Science*, 382, eadi5177, <https://doi.org/10.1126/science.ad5177>, 2023.

585 585 Inglis, G. N., Bragg, F., Burls, N. J., Cramwinckel, M. J., Evans, D., Foster, G. L., Huber, M., Lunt, D. J., Siler, N., Steinig, S., Tierney, J. E., Wilkinson, R., Anagnostou, E., de Boer, A. M., Dunkley Jones, T., Edgar, K. M., Hollis, C. J., Hutchinson, D. K., and Pancost, R. D.: Global mean surface temperature and climate sensitivity of the early Eocene Climatic Optimum (EECO), Paleocene–Eocene Thermal Maximum (PETM), and latest Paleocene, *Climate of the Past*, 16, 1953–1968, <https://doi.org/10.5194/cp-16-1953-2020>, 2020a.

Inglis, G. N., Rohrissen, M., Kennedy, E. M., Crouch, E. M., Raine, J. I., Strogen, D. P., Naafs, B. D. A., Collinson, M. E., and Pancost, R. D.: Terrestrial methane cycle perturbations during the onset of the Paleocene-Eocene Thermal Maximum, *Geology*, 49, 520–524, <https://doi.org/10.1130/G48110.1>, 2020b.

Kaplan, J. O., Bigelow, N. H., Prentice, I. C., Harrison, S. P., Bartlein, P. J., Christensen, T. R., Cramer, W., Matveyeva, N. V., McGuire, A. D., Murray, D. F., Razzhivin, V. Y., Smith, B., Walker, D. A., Anderson, P. M., Andreev, A. A., Brubaker, L. B., Edwards, M. E., and Lozhkin, A. V.: Climate change and Arctic ecosystems: 2. Modeling, paleodata-model comparisons, and future projections, *Journal of Geophysical Research: Atmospheres*, 108, [https://doi.org/https://doi.org/10.1029/2002JD002559](https://doi.org/10.1029/2002JD002559), 2003.

595 595 Kelemen, F. D., Steinig, S., de Boer, A., Zhu, J., Chan, W.-L., Niezgodzki, I., Hutchinson, D. K., Knorr, G., Abe-Ouchi, A., and Ahrens, B.: Meridional Heat Transport in the DeepMIP Eocene Ensemble: Non-CO₂ and CO₂ Effects, *Paleoceanography and Paleoclimatology*, 38, e2022PA004607, <https://doi.org/https://doi.org/10.1029/2022PA004607>, e2022PA004607 2022PA004607, 2023.



Kiehl, J. T. and Shields, C. A.: Sensitivity of the Palaeocene-Eocene Thermal Maximum climate to cloud properties, *Philosophical Transactions of the Royal Society A: Mathematical, Physical and Engineering Sciences*, 371, 20–20130 093, 2013.

600 Ladant, J.-B., Millot-Weil, J., de Lavergne, C., Green, J. A. M., Nguyen, S., and Donnadieu, Y.: The Role of Tidal Mixing in Shaping Early Eocene Deep Ocean Circulation and Oxygenation, *Paleoceanography and Paleoceanography*, 39, e2023PA004 822, <https://doi.org/https://doi.org/10.1029/2023PA004822> e2023PA004822, 2024.

Loptson, C. A., Lunt, D. J., and Francis, J. E.: Investigating vegetation-climate feedbacks during the early Eocene, *Climate of the Past*, 10, 419–436, <https://doi.org/10.5194/cp-10-419-2014>, 2014.

605 Lunt, D.: Code for DeepMIP-Eocene Phase2 Exp Design GMD paper, <https://doi.org/10.5281/zenodo.17887456>, 2025a.

Lunt, D.: Files for DeepMIP-Eocene Phase2 Exp Design GMD paper, <https://doi.org/10.5281/zenodo.17889194>, 2025b.

Lunt, D. J., Ridgwell, A., Valdes, P. J., and Seale, A.: “Sunshade World”: A fully coupled GCM evaluation of the climatic impacts of geoengineering, *Geophysical Research Letters*, 35, <https://doi.org/https://doi.org/10.1029/2008GL033674>, 2008.

610 Lunt, D. J., Huber, M., Anagnostou, E., Baatsen, M. L. J., Caballero, R., DeConto, R., Dijkstra, H. A., Donnadieu, Y., Evans, D., Feng, R., Foster, G. L., Gasson, E., von der Heydt, A. S., Hollis, C. J., Inglis, G. N., Jones, S. M., Kiehl, J., Kirtland Turner, S., Korty, R. L., Kozdon, R., Krishnan, S., Ladant, J.-B., Langebroek, P., Lear, C. H., LeGrande, A. N., Littler, K., Markwick, P., Otto-Bliesner, B., Pearson, P., Poulsen, C. J., Salzmann, U., Shields, C., Snell, K., Stärz, M., Super, J., Tabor, C., Tierney, J. E., Tourte, G. J. L., Tripati, A., Upchurch, G. R., Wade, B. S., Wing, S. L., Winguth, A. M. E., Wright, N. M., Zachos, J. C., and Zeebe, R. E.: The DeepMIP contribution to PMIP4: experimental design

615 for model simulations of the EECO, PETM, and pre-PETM (version 1.0), *Geoscientific Model Development*, 10, 889–901, <https://doi.org/10.5194/gmd-10-889-2017>, 2017.

Lunt, D. J., Bragg, F., Chan, W.-L., Hutchinson, D. K., Ladant, J.-B., Morozova, P., Niezgodzki, I., Steinig, S., Zhang, Z., Zhu, J., Abe-620 Ouchi, A., Anagnostou, E., de Boer, A. M., Coxall, H. K., Donnadieu, Y., Foster, G., Inglis, G. N., Knorr, G., Langebroek, P. M., Lear, C. H., Lohmann, G., Poulsen, C. J., Sepulchre, P., Tierney, J. E., Valdes, P. J., Volodin, E. M., Dunkley Jones, T., Hollis, C. J., Huber, M., and Otto-Bliesner, B. L.: DeepMIP: model intercomparison of early Eocene climatic optimum (EECO) large-scale climate features and comparison with proxy data, *Climate of the Past*, 17, 203–227, <https://doi.org/10.5194/cp-17-203-2021>, 2021.

Markwick, P. J.: The palaeogeographic and palaeoclimatic significance of climate proxies for data-model comparisons, in: Deep time perspectives on climate change: marrying the signal from computer models and biological proxies, edited by M. M. W., Haywood, A. M., Gregory, J. F., and Schmidt, D. N., The Micropalaeontological Society Special Publications, Geological Society of London, 2007.

625 Meijer, N., Licht, A., Woutersen, A., Hoorn, C., Robin-Champigneul, F., Rohrmann, A., Tagliavento, M., Brugger, J., Kelemen, F. D., Schauer, A. J., Hren, M. T., Sun, A., Fiebig, J., Mulch, A., and Dupont-Nivet, G.: Proto-monsoon rainfall and greening in Central Asia due to extreme early Eocene warmth, *Nature geoscience*, 17, 158–164, 2024.

Meinshausen, M., Vogel, E., Nauels, A., Lorbacher, K., Meinshausen, N., Etheridge, D. M., Fraser, P. J., Montzka, S. A., Rayner, P. J., Trudinger, C. M., Krummel, P. B., Beyerle, U., Canadell, J. G., Daniel, J. S., Enting, I. G., Law, R. M., Lunder, C. R., O'Doherty, S., 630 Prinn, R. G., Reimann, S., Rubino, M., Velders, G. J. M., Vollmer, M. K., Wang, R. H. J., and Weiss, R.: Historical greenhouse gas concentrations for climate modelling (CMIP6), *Geoscientific Model Development*, 10, 2057–2116, <https://doi.org/10.5194/gmd-10-2057-2017>, 2017.

Meinshausen, M., Nicholls, Z. R. J., Lewis, J., Gidden, M. J., Vogel, E., Freund, M., Beyerle, U., Gessner, C., Nauels, A., Bauer, N., Canadell, J. G., Daniel, J. S., John, A., Krummel, P. B., Luderer, G., Meinshausen, N., Montzka, S. A., Rayner, P. J., Reimann, S., Smith, S. J., van den



635 Berg, M., Velders, G. J. M., Vollmer, M. K., and Wang, R. H. J.: The shared socio-economic pathway (SSP) greenhouse gas concentrations and their extensions to 2500, *Geoscientific Model Development*, 13, 3571–3605, <https://doi.org/10.5194/gmd-13-3571-2020>, 2020.

Merdith, A. S., Williams, S. E., Collins, A. S., Tetley, M. G., Mulder, J. A., Blades, M. L., Young, A., Armistead, S. E., Cannon, J., Zahirovic, S., and Müller, R. D.: Extending full-plate tectonic models into deep time: Linking the Neoproterozoic and the Phanerozoic, *Earth-Science Reviews*, 214, 103 477, [https://doi.org/https://doi.org/10.1016/j.earscirev.2020.103477](https://doi.org/10.1016/j.earscirev.2020.103477), 2021.

640 Montheil, L., Licht, A., Beard, K. C., Métais, G., Coster, P., Vaes, B., Donnadieu, Y., Pineau, E., Husson, L., and Dupont-Nivet, G.: Across ancient oceans: Eocene dispersal routes of Asian terrestrial mammals to Europe, Afro-Arabia and South America, *Earth-Science Reviews*, 273, 105 352, <https://doi.org/https://doi.org/10.1016/j.earscirev.2025.105352>, 2026.

Müller, R. D., Sdrolias, M., Gaina, C., and Roest, W. R.: Age, spreading rates, and spreading asymmetry of the world's ocean crust, *Geochemistry, Geophysics, Geosystems*, 9, <https://doi.org/https://doi.org/10.1029/2007GC001743>, 2008.

645 Müller, R. D., Cannon, J., Qin, X., Watson, R. J., Gurnis, M., Williams, S., Pfaffelmoser, T., Seton, M., Russell, S. H. J., and Zahirovic, S.: GPlates: Building a Virtual Earth Through Deep Time, *Geochemistry, Geophysics, Geosystems*, 19, 2243–2261, <https://doi.org/https://doi.org/10.1029/2018GC007584>, 2018.

National Geophysical Data Center: 5-minute Gridded Global Relief Data (ETOPO5), <https://doi.org/doi:10.7289/V5D798BF>, 1993.

Niezgodzki, I., Knorr, G., Lohmann, G., Lunt, D. J., Poulsen, C. J., Steinig, S., Zhu, J., de Boer, A., Chan, W.-L., Don-650 nadieu, Y., Hutchinson, D. K., Ladant, J.-B., and Morozova, P.: Simulation of Arctic sea ice within the DeepMIP Eocene ensemble: Thresholds, seasonality and factors controlling sea ice development, *Global and Planetary Change*, 214, 103 848, <https://doi.org/https://doi.org/10.1016/j.gloplacha.2022.103848>, 2022.

Nooteboom, P. D., Baatsen, M., Bijl, P. K., Kliphuis, M. A., van Sebille, E., Sluijs, A., Dijkstra, H. A., and von der Heydt, A. S.: Improved Model-Data Agreement With Strongly Eddying Ocean Simulations in the Middle-Late Eocene, *Paleoceanography and Paleoclimatology*, 37, e2021PA004 405, <https://doi.org/https://doi.org/10.1029/2021PA004405>, e2021PA004405 2021PA004405, 2022.

655 O'Neill, C., Müller, D., and Steinberger, B.: On the uncertainties in hot spot reconstructions and the significance of moving hot spot reference frames, *Geochemistry, Geophysics, Geosystems*, 6, 2005.

Paxman, G. J., Jamieson, S. S., Hochmuth, K., Gohl, K., Bentley, M. J., Leitchenkov, G., and Ferraccioli, F.: Reconstructions of Antarctic topography since the Eocene–Oligocene boundary, *Palaeogeography, Palaeoclimatology, Palaeoecology*, 535, 109 346, <https://doi.org/https://doi.org/10.1016/j.palaeo.2019.109346>, 2019.

Poblete, F., Dupont-Nivet, G., Licht, A., van Hinsbergen, D., Roperch, P., Mihalynuk, M., Johnston, S., Guillocheau, F., Baby, G., Fluteau, F., Robin, C., van der Linden, T., Ruiz, D., and Baatsen, M.: Towards interactive global paleogeographic maps, new reconstructions at 60, 40 and 20Ma, *Earth-Science Reviews*, 214, 103 508, <https://doi.org/https://doi.org/10.1016/j.earscirev.2021.103508>, 2021.

Pound, M. J., Tindall, J., Pickering, S. J., Haywood, A. M., Dowsett, H. J., and Salzmann, U.: Late Pliocene lakes and soils: a global data set 665 for the analysis of climate feedbacks in a warmer world, *Climate of the Past*, 10, 167–180, <https://doi.org/10.5194/cp-10-167-2014>, 2014.

Rae, J. W., Zhang, Y. G., Liu, X., Foster, G. L., Stoll, H. M., and Whiteford, R. D.: Atmospheric CO₂ over the Past 66 Million Years from Marine Archives, *Annual Review of Earth and Planetary Sciences*, 49, 609–641, <https://doi.org/10.1146/annurev-earth-082420-063026>, 2021.

Rak, J.: Because It Is There? Mount Everest, Masculinity, and the Body of George Mallory, *The International Journal of the History of Sport*, 670 38, 157–183, <https://doi.org/10.1080/09523367.2020.1854738>, 2021.



Reichgelt, T., Greenwood, D. R., Steinig, S., Conran, J. G., Hutchinson, D. K., Lunt, D. J., Scriven, L. J., and Zhu, J.: Plant Proxy Evidence for High Rainfall and Productivity in the Eocene of Australia, *Paleoceanography and Paleoclimatology*, 37, e2022PA004418, <https://doi.org/10.1029/2022PA004418>, e2022PA004418 2022PA004418, 2022.

Ross, P.: Deep ocean circulation during the early Eocene: a model-data comparison, Ph.D. thesis, Imperial College, University of London, 675 2023.

Sagoo, N., Valdes, P., Flecker, R., and Gregoire, L.: The Early Eocene equitable climate problem: can perturbations of climate model parameters identify possible solutions?, *Philosophical Transactions of the Royal Society A: Mathematical, Physical and Engineering Sciences*, 317, <https://doi.org/10.1098/rsta.2013.0123>, 2013.

Salzmann, U., Haywood, A. M., Lunt, D. J., Valdes, P. J., and Hill, D. J.: A new global biome reconstruction and data-model comparison for 680 the Middle Pliocene, *Global Ecology and Biogeography*, 17, 432–447, <https://doi.org/10.1111/j.1466-8238.2008.00381.x>, 2008.

Scotese, C. R. and Wright, N.: PALEOMAP Paleodigital Elevation MOdels (PaleoDEMs) for the Phanerozoic PALEOMAP Project, Earthbyte, <https://www.earthbyte.org/paleodem-resource-scotese-and-wright-2018>, [Online; accessed 30th June 2018], 2018.

Shields, C. A., Kiehl, J. T., Rush, W., Rothstein, M., and Snyder, M. A.: Atmospheric rivers in high-resolution simulations of the Paleocene Eocene Thermal Maximum (PETM), *Palaeogeography, Palaeoclimatology, Palaeoecology*, 567, 110293, 685 <https://doi.org/10.1016/j.palaeo.2021.110293>, 2021.

Smith, B., Wårliind, D., Arneth, A., Hickler, T., Leadley, P., Siltberg, J., and Zaehle, S.: Implications of incorporating N cycling and N limitations on primary production in an individual-based dynamic vegetation model, *Biogeosciences*, 11, 2027–2054, <https://doi.org/10.5194/bg-11-2027-2014>, 2014.

690 Spicer, R. A., Farnsworth, A., Su, T., Ding, L., Witkowski, C. R., Li, S.-F., Xiong, Z., Zhou, Z., Li, S., Hughes, A. C., Valdes, P. J., Widdowson, M., Zhang, X., He, S., Liu, J., Huang, J., Herman, A. B., Xu, Q., Liu, X., Jin, J., Pancost, R. D., Lunt, D. J., and Zhang, S.: The progressive co-evolutionary development of the Pan-Tibetan Highlands, the Asian monsoon system and Asian biodiversity, *Geological Society, London, Special Publications*, 549, 55–112, <https://doi.org/10.1144/SP549-2023-180>, 2025.

Steinig, S., Abe-Ouchi, A., de Boer, A., Chan, W.-L., Donnadieu, Y., Hutchinson, D., Knorr, G., Ladant, J.-B., Morozova, P., Niezgodzki, 695 I., Poulsen, C., Volodin, E., Zhang, Z., Zhu, J., Evans, D., Inglis, G., Meckler, A. N., and Lunt, D.: DeepMIP-Eocene-p1: multi-model dataset and interactive web application for Eocene climate research, *Scientific Data*, 11, <https://doi.org/10.1038/s41597-024-03773-4>, 2024.

Steinig, S., Williams, C., Burls, N. J., Cramwinckel, M. J., Farnsworth, A., Foster, G., Hopcroft, P., Inglis, G., Lear, C., Osprey, A., Pancost, 700 Roberts, W., Selar, A., Stone, E., Wood, R., Zhi, J., and Lunt, D.: Super warm early Eocene simulations with HadGEM3-GC31-LL, *Journal of Geophysical Research: Atmospheres*, -, in prep.

Straume, E., Gaina, C., Medvedev, S., and Nisancioglu, K.: Global Cenozoic Paleobathymetry with a focus on the Northern Hemisphere Oceanic Gateways, *Gondwana Research*, 86, 126–143, <https://doi.org/10.1016/j.gr.2020.05.011>, 2020.

Straume, E. O., Steinberger, B., Becker, T. W., and Faccenna, C.: Impact of mantle convection and dynamic topography on the Cenozoic paleogeography of Central Eurasia and the West Siberian Seaway, *Earth and Planetary Science Letters*, 630, 118615, 705 <https://doi.org/10.1016/j.epsl.2024.118615>, 2024.

Tetley, M. G., Williams, S. E., Gurnis, M., Flament, N., and Müller, R. D.: Constraining Absolute Plate Motions Since the Triassic, *Journal of Geophysical Research: Solid Earth*, 124, 7231–7258, <https://doi.org/10.1029/2019JB017442>, 2019.



Thompson, N., Salzmann, U., Hutchinson, D. K., Strother, S. L., Pound, M. J., Utescher, T., Brugger, J., Hickler, T., Hocking, E. P., and Lunt, D. J.: Global vegetation zonation and terrestrial climate of the warm Early Eocene, *Earth-Science Reviews*, 261, 105 036, 710 <https://doi.org/https://doi.org/10.1016/j.earscirev.2024.105036>, 2025.

Torsvik, T. H., Van der Voo, R., Preeden, U., Mac Niocaill, C., Steinberger, B., Doubrovine, P. V., Van Hinsbergen, D. J., Domeier, M., Gaina, C., Tohver, E., et al.: Phanerozoic polar wander, palaeogeography and dynamics, *Earth-Science Reviews*, 114, 325–368, 2012.

West, C. K., Greenwood, D. R., Reichgelt, T., Lowe, A. J., Vachon, J. M., and Basinger, J. F.: Paleobotanical proxies for early Eocene climates and ecosystems in northern North America from middle to high latitudes, *Climate of the Past*, 16, 1387–1410, <https://doi.org/10.5194/cp-16-1387-2020>, 2020.

715 Westerweel, J., Roperch, P., Win, Z., and Dupont-Nivet, G.: Northward drift of the Burma Terrane with India during the Cenozoic and implications for the India–Asia collision, *Geological Society, London, Special Publications*, 549, 11–54, <https://doi.org/10.1144/SP549-2024-18>, 2025.

Willard, D. A., Donders, T. H., Reichgelt, T., Greenwood, D. R., Sangiorgi, F., Peterse, F., Nierop, K. G., Frieling, J., Schouten, S., and Sluijs, 720 A.: Arctic vegetation, temperature, and hydrology during Early Eocene transient global warming events, *Global and Planetary Change*, 178, 139–152, <https://doi.org/https://doi.org/10.1016/j.gloplacha.2019.04.012>, 2019.

Williams, C. J. R., Lunt, D. J., Salzmann, U., Reichgelt, T., Inglis, G. N., Greenwood, D. R., Chan, W.-L., Abe-Ouchi, A., Donnadieu, Y., Hutchinson, D. K., de Boer, A. M., Ladant, J.-B., Morozova, P. A., Niegzodzki, I., Knorr, G., Steinig, S., Zhang, Z., Zhu, J., Huber, M., and Otto-Bliesner, B. L.: African Hydroclimate During the Early Eocene From the DeepMIP Simulations, *Paleoceanography and 725 Paleoclimatology*, 37, e2022PA004419, <https://doi.org/https://doi.org/10.1029/2022PA004419>, e2022PA004419 2022PA004419, 2022.

Wilson, D. S., Jamieson, S. S., Barrett, P. J., Leitchenkov, G., Gohl, K., and Larter, R. D.: Antarctic topography at the Eocene–Oligocene boundary, *Palaeogeography, Palaeoclimatology, Palaeoecology*, 335–336, 24–34, <https://doi.org/https://doi.org/10.1016/j.palaeo.2011.05.028>, *Cenozoic Evolution of Antarctic Climates, Oceans and Ice Sheets*, 2012.

730 Wilton, D. J., Badger, M. P. S., Kantzas, E. P., Pancost, R. D., Valdes, P. J., and Beerling, D. J.: A predictive algorithm for wetlands in deep time paleoclimate models, *Geoscientific Model Development*, 12, 1351–1364, <https://doi.org/10.5194/gmd-12-1351-2019>, 2019.

Wright, N. M., Seton, M., Williams, S. E., Whittaker, J. M., and Müller, R. D.: Sea-level fluctuations driven by changes in global ocean basin volume following supercontinent break-up, *Earth-Science Reviews*, 208, 103 293, <https://doi.org/https://doi.org/10.1016/j.earscirev.2020.103293>, 2020.

Zahirovic, S., Eleish, A., Doss, S., Pall, J., Cannon, J., Pistone, M., Tetley, M. G., Young, A., and Fox, P.: Subduction and carbonate platform 735 interactions, *Geoscience Data Journal*, 9, 371–383, <https://doi.org/https://doi.org/10.1002/gdj3.146>, 2022.

Zhang, Y., de Boer, A. M., Lunt, D. J., Hutchinson, D. K., Ross, P., van de Flierdt, T., Sexton, P., Coxall, H. K., Steinig, S., Ladant, J.-B., Zhu, J., Donnadieu, Y., Zhang, Z., Chan, W.-L., Abe-Ouchi, A., Niegzodzki, I., Lohmann, G., Knorr, G., Poulsen, C. J., and Huber, M.: Early Eocene Ocean Meridional Overturning Circulation: The Roles of Atmospheric Forcing and Strait Geometry, *Paleoceanography and 740 Paleoclimatology*, 37, e2021PA004329, <https://doi.org/https://doi.org/10.1029/2021PA004329>, e2021PA004329 2021PA004329, 2022.

Zhang, Y., de Boer, A. M., Qin, G., Lunt, D. J., Hutchinson, D. K., Steinig, S., Niegzodzki, I., Wade, B. S., Liu, X., Poulsen, C. J., and Lohmann, G.: Poleward expansion of North Pacific gyre circulation during the warm early Eocene inferred from inter-model comparisons, *Palaeogeography, Palaeoclimatology, Palaeoecology*, 661, 112 712, <https://doi.org/https://doi.org/10.1016/j.palaeo.2024.112712>, 2025.

Zhang, Z., Zhang, Z., Nummelin, A., Straume, E. O., Meckler, A. N., Langebroek, P. M., He, Z., Tan, N., and Guo, Z.: Influence of plate reference frames on deep-time climate simulations, *Global and Planetary Change*, 233, 104 352, 745 <https://doi.org/https://doi.org/10.1016/j.gloplacha.2023.104352>, 2024.



Zhu, J., Poulsen, C. J., and Tierney, J. E.: Simulation of Eocene extreme warmth and high climate sensitivity through cloud feedbacks, *Science advances*, 5, eaax1874, 2019.

Zhu, J., Poulsen, C. J., Otto-Bliesner, B. L., Liu, Z., Brady, E. C., and Noone, D. C.: Simulation of early Eocene water isotopes using an Earth system model and its implication for past climate reconstruction, *Earth and Planetary Science Letters*, 537, 116 164, 2020.

750 Zhu, J., Poulsen, C. J., and Otto-Bliesner, B. L.: Modeling Past Hothouse Climates as a Means for Assessing Earth System Models and Improving the Understanding of Warm Climates, *Annual Review of Earth and Planetary Sciences*, 52, 2024.



Table 1. Summary of simulations associated with DeepMIP-Eocene Phase 2, including two mandatory relevant simulations from CMIP7 (*piControl* and *abrupt-4×CO₂*), the mandatory two standard simulations (*deepmip-p2-stand-5xCO₂* and *deepmip-p2-stand-1xCO₂*), and some of the suggested sensitivity studies. Mandatory simulations are in **bold**.

Simulation Name	Simulation description	CO ₂ [ppmv]	paleogeog.	vegetation	S ₀	CH ₄ [ppnb]
<i>piControl</i>	preindustrial control	280^[1]	modern	modern	modern	800^[2]
<i>abrupt-4×CO₂</i>	abrupt increase to 4×PI	1120	modern	modern	modern	800
<i>deepmip-p2-stand-5×CO₂</i>	EECO, at 5×PI	1400	51 Ma	this study	modern	800
<i>deepmip-p2-stand-1×CO₂</i>	EECO, at 1×PI	280	51 Ma	this study	modern	800
<i>deepmip-p2-sens-5×CO₂-thompson</i>	sensitivity study to prescribed vegetation	1400	51 Ma	Thompson et al. (2025)	modern	800
<i>deepmip-p2-sens-5×CO₂-solarmethane</i>	sensitivity study to solar and methane	1400	51 Ma	this study	51 Ma	3000
<i>deepmip-p2-sens-5×CO₂-paleogeography</i>	sensitivity study to prescribed paleogeography; Herold et al. (2014) on Phase 2 reference frame	1400	modified	this study	modern	800
<i>deepmip-p2-sens-Y×CO₂</i>	sensitivity study to prescribed CO ₂ at 51 Ma. Y=2,3,4,6,9	Y×PI	51 Ma	this study	modern	800
<i>equilibrium-4×CO₂</i>	equilibrium at 4×PI	1120	modern	modern	modern	800

^[1] If a value different from 280 ppmv is used for *piControl*, then all other CO₂ values in the table should be changed accordingly, as a ratio. Note that Meinshausen et al. (2017) suggests 284.3 ppmv for CMIP6 *piControl* simulations.

^[2] If a value different from 800 ppbv is used for *piControl*, then all other CH₄ values in the table should be changed accordingly, as a ratio. Note that Meinshausen et al. (2017) suggests 808.2 ppbv for CMIP6 *piControl* simulations.